5-2019

Human Powered Energy Harvester based on Autowinder Mechanism: Analysis, Build and Test

Abby Joseph Arakal George
Clemson University, abbyjgeorge@gmail.com

HUMAN POWERED ENERGY HARVESTER BASED ON AUTOWINDER MECHANISM: ANALYSIS, BUILD AND TEST

A Thesis
Presented to
the Graduate School of
Clemson University

In Partial Fulfillment
of the Requirements for the Degree
Master of Science
Mechanical Engineering

---

by
Abby Joseph Arakal George
May 2019

Accepted by:
Dr. John R. Wagner, Committee Chair
Dr. Todd Schweisinger
Dr. Gregory Mocko

ABSTRACT

Experts estimate that approximately one third of the worldwide population currently owns a smartphone, and subscriptions continue to grow. Compared to mobile devices of the past decade, smartphones provide desktop computer-level processing power in a palm-sized package. However, the high computing power and 24 hours - 7 days a week connectivity results in a shorter battery life, often forcing the user to rely on portable battery packs. Worldwide energy consumption statistics show that the electric power grid depends primarily on fossil fuels. Thus, a renewable power source based on human motion energy harvesting offers a potential solution to power portable communication devices and may help reduce dependence on the power grid.

A novel wrist-worn energy-harvester, based on an automatic winding mechanism, was designed, fabricated and experimentally tested. The mechanism frequently employed in wrist and pocket watches dates back to the 18^{th} century, and is one of the oldest examples of mobile human energy harvesting. In this project, the prototype device contains a rotary pendulum connected to a DC generator through a planetary gear train. An electronics module consisting of a rectifier and boost converter filters the generator output, supplying regulated DC output to charge a battery, and/or power an electrical load. An onboard microcontroller broadcasts the voltage, current, and power data wirelessly for data collection during testing.

Numerical and experimental validations were conducted for the energy harvester. A mathematical model for human arm swing dynamics was developed based on a triple pendulum system, and the device's behavior was studied for both walking and running

activities. The mechanical energy output from the rotary harvester pendulum was predicted to be 0.42 mJ and 2.06 mJ for simulated walking and running sequences over a period of 5 seconds (without load). A subsequent mathematical model was developed incorporating the electromechanical behavior of the generator and attached electronics module. A simulated running sequence with a representative electrical load yielded 1.72 mJ of electrical energy output over 5 seconds. The prototype was experimentally validated over the same conditions, resulting in an unregulated energy output of 1.39 mJ and a regulated energy output at 5 VDC of 1.16mJ for 5 seconds. Experimental testing successfully demonstrated the harvester's potential as a mobile energy source for portable consumer electronics. Future steps shall focus on implementing efficient components for increased power output and designing for improved ergonomics.

DEDICATION

I dedicate this thesis to my family members, for being the three strong pillars throughout my life, and for encouraging and supporting me to pursue my master's degree at Clemson University.

ACKNOWLEDGMENTS

I would like to thank Dr. John R. Wagner for his mentorship and support throughout my program. His emphasis on quality of work and effective communication has helped me to expand my skills and prepare me for the engineering industry. I appreciate my committee members Dr. Gregory Mocko and Dr. Todd Schweisinger for their valuable support with various phases of my research. I thank Mr. Michael Justice for his help and inputs with identifying components and machining parts. Finally, I would like to thank Mr. David Moline for his help with proof reading the research papers.

TABLE OF CONTENTS

Page

Table of Contents (Continued) Page

LIST OF TABLES

LIST OF FIGURES

List of Figures (Continued)

Page

List of Figures (Continued)

Page

NOMENCLATURE

a	Upper arm maximum torque (N.m)
A_n	Grouped inertia term
B_{ij}	Grouped inertia term
$\boldsymbol{C}$	Damping matrix
c_1	Viscous damping coefficient for upper arm (N.m.s)
c_2	Viscous damping coefficient for lower arm (N.m.s)
c_3	Effective viscous damping at third pivot (N.m.s)
C_G	Viscous damping coefficient for generator (N.m.s)
c_P	Viscous damping coefficient for pendulum (N.m.s)
e_1	Distance of centroid of upper arm from pivot (m)
e_2	Distance of centroid of lower arm from pivot (m)
e_3	Distance of centroid of harvester rotor from pivot (m)
$\boldsymbol{F_E(t)}$	Time dependent excitation matrix
f	Frequency of torque input for upper arm (Hz)
f_r	Frequency of upper arm torque for running (Hz)
f_w	Frequency of upper arm torque for walking (Hz)
g	Acceleration due to gravity ($m.s^{-2}$)
i_A	Generator armature current (Ampere)
I_1	Mass moment of inertia of upper arm ($kg.m^2$)
I_2	Mass moment of inertia of lower arm ($kg.m^2$)

I_3	Effective mass moment of inertia at third pivot (kg.m^2)
I_P	Mass moment of inertia of harvester pendulum (kg.m^2)
I_{RG}	Mass moment of inertia of ring gear (kg.m^2)
I_{PG}	Mass moment of inertia of pinion gear (kg.m^2)
J_G	Mass moment of inertia of generator (kg.m^2)
k_E	Generator back-emf constant (V.rad^{-1}.sec^{-1})
k_T	Generator torque constant (N.m.Amp^{-1})
l_1	Length of upper arm (m)
l_2	Length of lower arm (m)
l_3	Radius of the harvester rotor (m)
L_G	Generator inductance (H)
m_1	Mass of upper pendulum (kg)
m_2	Mass of lower pendulum (kg)
m_3	Mass of the harvester rotor (kg)
N_{PG}	Number of teeth of pinion gear
N_{RG}	Number of teeth of ring gear
$\boldsymbol{M}(\boldsymbol{\theta})$	State dependent inertia matrix
$M_{E1}(t)$	Time dependent moment at upper arm joint (N.m)
$M_{E2}(t)$	Constant torque at lower arm joint (N.m)
$\boldsymbol{N}(\boldsymbol{\theta})$	State dependent non-linearity matrix
$\boldsymbol{p}(\boldsymbol{\theta})$	State dependent energy matrix

P_E	Electrical power generated by the harvester (W)
P_M	Mechanical power generated by the harvester (W)
q	Electric charge (Coulomb)
q_{1r}	Maximum torque at upper arm for running (N.m)
q_{2r}	Maximum torque at lower arm for running (N.m)
q_{1w}	Maximum torque at upper arm for walking (N.m)
q_{2w}	Maximum torque at lower arm for walking (N.m)
q_n	Generalized coordinates
Q_n	Generalized forces
r_1	Radius of first cylindrical pendulum (m)
r_2	Radius of second cylindrical pendulum (m)
R_G	Armature resistance (Ohm)
R_L	Load resistance (Ohm)
R_T	Total resistance (Ohm)
t	Time (sec)
T	Potential energy of the system (J)
U_n	Grouped potential energy term
V	Kinetic energy of the system (J)
x_1	X-coordinate of centroid of upper arm (m)
x_2	X-coordinate of centroid of lower arm (m)
x_3	X-coordinate of centroid of harvester rotor (m)

y_1	Y-coordinate of centroid of upper arm (m)
y_2	Y-coordinate of centroid of lower arm (m)
y_3	Y-coordinate of centroid of harvester rotor (m)
θ_1	Angle of upper arm with the vertical (rad)
θ_2	Angle of lower arm with the vertical (rad)
θ_3	Angle of harvester rotor with the vertical (rad)
τ_G	Generator torque (N.m)
τ_M	Torque generated by the harvester (N.m)
τ_P	Torque acting on the pendulum (N.m)
ω_M	Angular velocity of the harvester (rad.s^{-1})

CHAPTER ONE: INTRODUCTION

1.1 Background

Electricity has become an indispensable energy source in society since the early 19th century, from electrifying houses and fueling the second industrial revolution back then to powering our smartphones and charging electric vehicles now. Among the various sources available to produce electricity, fossil fuels such as coal and natural gas have been dominating worldwide power generation for the past decades as shown in Figure 1.1 (BP Statistical Review of World Energy, 2018). Studies on climate change suggest a strong correlation to fossil fuel consumption, with greenhouse gas emissions from these sources being one of the primary concerns due to their heavy impact on global temperature rise. Although environmentally friendly sources such as hydroelectric, solar and wind are available and being adopted in various scales worldwide; governmental policies, infrastrucutral challenges, geographical and economical factors often impede mass adoption of such renewable energy sources. In most cases, the required hardware is too expensive or inaccessible for communities in remote and developing areas.

Meanwhile, portable communication devices such as smartphones, smartwatches and tablets are becoming increasingly popular worldwide with a predicted userbase of 3 billion, or more than a third of the population by end of the year 2018 (Business Insider, 2018). Eventhough they offer users high computing and entertainment capabilities in a compact package, the battery life is often not an attractive selling point. Over the years, battery technology has not made the same advancement compared to CPU performance,

Figure 1.2 displays this trend (Starner, 1996). This often forces the user to carry portable power banks required to be charged separately, which may be cumbersome. A portable renewable energy source can offer the user with flexibility and independence from the power grid to power their portable devices. From a global energy consumption standpoint, using a portable renewable energy source as an alternative to supply power to the growing number of smartphones would have the potential to create a significant impact in reducing gross carbon footprint.

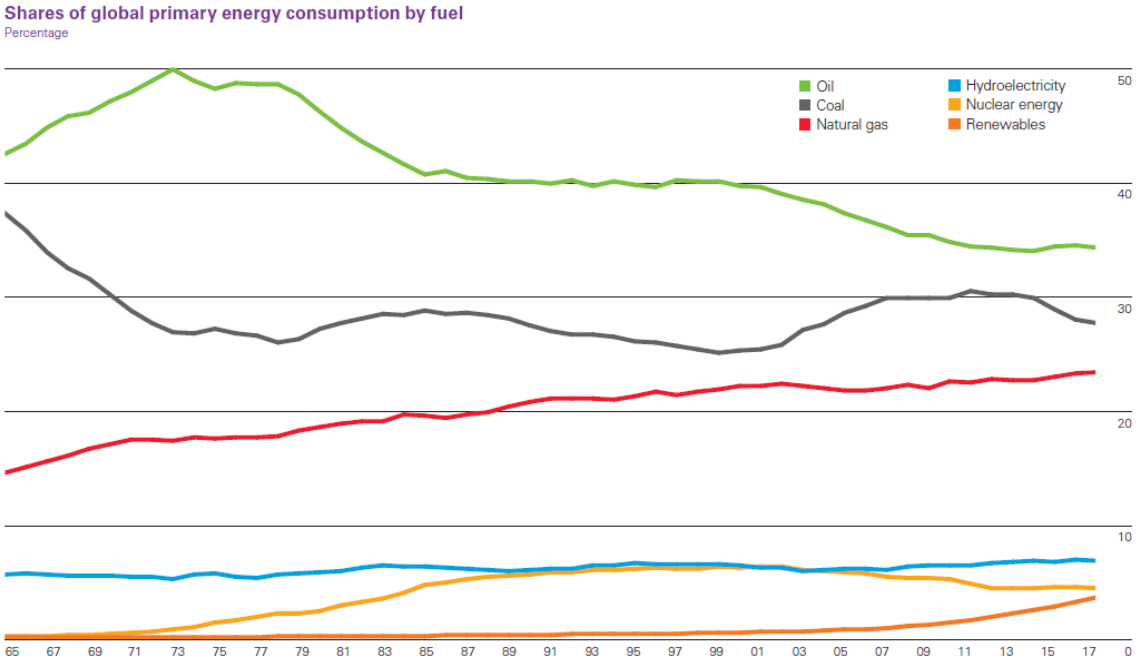

Figure 1.1: Global usage of energy sources including fossil fuels and renewables (BP Statistical Review of World Energy, 2018)

1.2 Human Energy Harvesting

Energy harvesting in general is the process by which energy required for an application may be extracted from the ambient sources, which are often renewable in

nature. Currently, portable solar mobile chargers are available in the market which lets a user charge their devices using compact solar panels (RavPower solar charger, 2018). While these solar chargers offer mobility, the need for sunlight and long turnaround time for charging due to the low power output of the solar panels undermines their usability. Hand cranking chargers are also available which requires the user to manually crank a handle connected to a small electric generator (K-Tor USB Hand Crank Generator, 2018). The device is able to power portable electronics although with active input from the user, which might be a disadavantage in terms on convenience. In this background, human energy harvesting using inertial methods can be a mobile yet flexible source of power. Inertial methods help to extracting energy passively, avoiding the need for active inputs and thereby providing a better user experience. The adoption of human energy harvesting technologies can be improved substantially by offering users a more convenient and mobile solution to charge portable electronic devices, enabling them to stay independent of the power grid.

Human energy harvesting for portable applications involves utilizing one or more of the various body sources such as body heat, impact motion from foot fall, inertial motion from limbs, and in some case even blood pressure. Figure 1.2 displays examples of human energy harvesting: (a) The Seiko Thermic Watch uses body heat to recharge it's batteries; (b) shoe mounted generator by Paradiso *et al.* (2001) is an example of impact energy harvesting of footfall, consisting of a geared generator actuated while human walking; and (c) the backpack mounted linear generator by Rome *et al.* (2005) utilizes the relative motion of the backpack with the user's body while walking or running activities due to

inertia. Finally, Figure 1.2 (d) shows an autowinder mechanism courtesy of Omega SA, an example of inertial energy harvesting using arm motion. Each method has its advantages and disadvantages, with inertial energy harvesting offering a good balance between power generation potential and ease of use. The autowinder mechanism can be easily integrated owing to its compact size and non intrusive operation, opening opportunities for scaling up the technology for larger power generation.

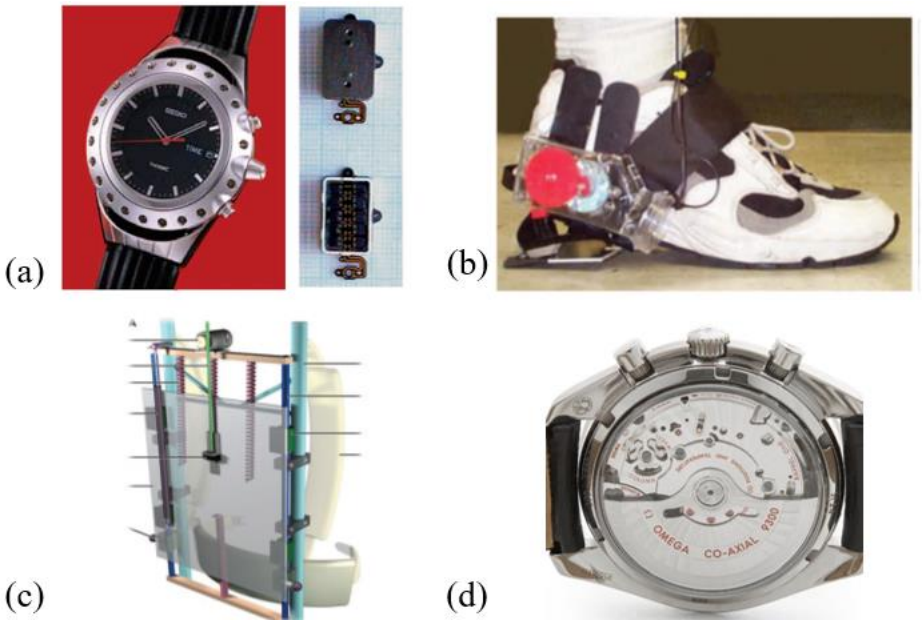

Figure 1.2: Examples for human energy harvesting: (a) Seiko Thermic Watch, (Seiko Watch Corporation, 2018), (b) Shoe-mounted Generator, Paradiso *et al.*, (2001), (c) Backpack-mounted generator, Rome *et al.*, (2005) and, (d) Omega Speedmaster auto-winding watch, (Omega SA, 2018)

1.3 Auto Winder Approach

The autowinder mechanism has been succesfully used in mechanical watches for over 200 years for automatically winding the main springs, and more recently, to recharge

watch batteries. Among the various methods that exist, inertial energy harvesting has the advantage of being able to extract energy from human body motion with relatively minimal active effort from the user. An ETA Swiss autowinder mechanism was studied to understand the working principle. A photograph of this arrangement is displayed in Figure 1.3, showing its main parts. It consists of a pendulum which may be excited by human arm motion, connected to an eccentric pawl lever. The pawl lever converts bidirectional rotation to unidirectional rotation turning the intermediate wheel, rewinding the main spring. In this research, the feasibility of scaling up this mechanism to generate more power for applications such as charging a smartphone, will be explored.

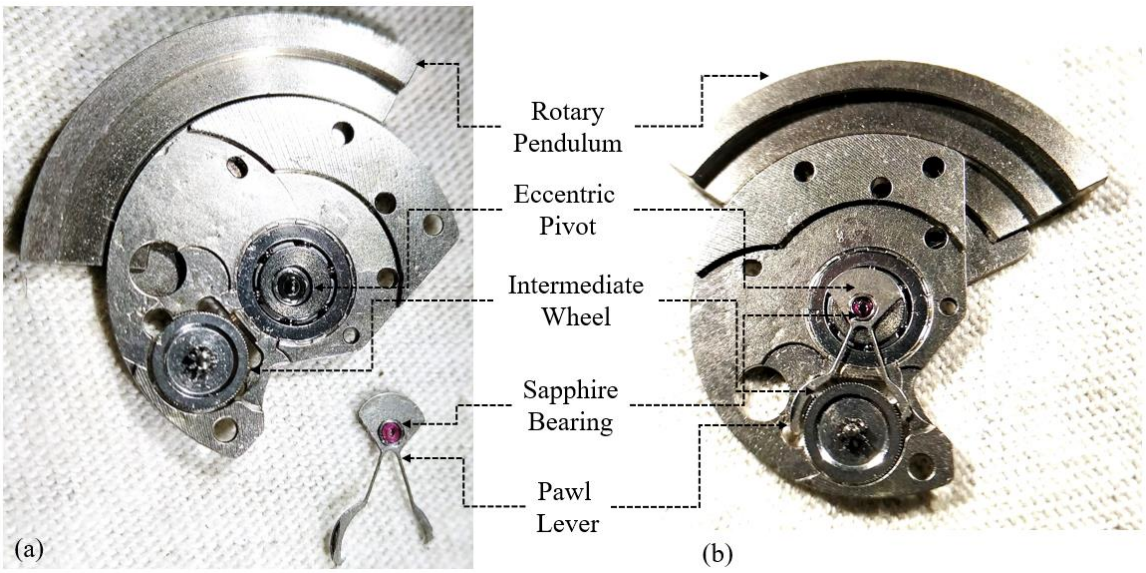

Figure 1.3: The ETA Autowinder mechanism: (a) Disassembled, and (b) Assembled

A novel human motion energy harvester based on the autowinder mechanism is proposed. This thesis presents the research conducted on the build, test and analysis of the energy harvester, as two chapters. Chapter 2 explains the initial mathematical model

developed to simulate arm motion dynamics for exciting a mobile energy harvester, and the predicted device behavior. The human arm-harvester system is modelled as a triple pendulum system acted on by time varying moments to emulate walking and running motions. The system response of the energy harvester is simulated with the mathematical model, predicting the maximum mechanical power output for each scenario. Chapter 3 elaborates the prototyping of the energy harvester, along with a mathematical model which describes the behavior of the combined electromechanical system of the harvester pendulum, DC generator, filtering circuits and electrical loads. Chapter 4 concludes the thesis with important findings and suggestions for future research. Appendices contain the MATLAB and Arduino code, photographs of the prototype harvester and it's components, and bill of materials.

CHAPTER TWO

ARM MOTION DYNAMICS TO EXCITE A MOBILE ENERGY HARVESTING AUTOWINDER

This chapter contains the preliminary numerical analysis and design of the energy harvester prototype. A mathematical model for simulating human arm dynamics and the mechanical behavior of the harvester pendulum is developed using the Lagrangian approach. Case studies were conducted to identify ideal conditions for excitation and maximize energy output. This chapter contains the preliminary numerical analysis and design of the energy harvester prototype.

2.1 Background

The proliferation of smartphone and smartwatch users worldwide has been pushing the research on extending the battery life and improving charging times. However, advanced computing power available owing to rapid developments in electronics adversely affects the battery life of such smart-devices. Within the past three decades, computational speed and memory capacity has improved a thousand fold, compared to just a five fold increase in energy density of batteries. Users have to resort to charging their devices frequently with portable battery packs used to extend battery life. Additional effort required to carry and charge these battery packs limit their usability, ultimately forcing the users to depend on the power grid to recharge their devices. Meanwhile, portable technologies that harvest energy from untapped sources in everyday life may be a convenient solution to frequent dependence on the grid for power needs. Among the various methods and sources

available, an energy harvesting system designed to generate electricity from human movements has great potential as a portable offline energy source.

The human body is a complex system presenting energy harvesting opportunities from sources such as body heat, breathing, blood pressure, and various modes of limb motion. Starner (1996) explored the energy harvesting potential of these sources to power portable electronics concluding that arm motion and footfalls had the highest rated potential for energy harvesting with 60W and 67W of power respectively. Shenck *et al.* (2001) investigated a flexible piezoelectric foil based shoe to harness sole-bending energy for powering wearable microelectronics. While footfalls or impact energy harvesting has great potential, harvesting usually requires modifying user's shoes, which may not be easily adopted. Breathing and body heat energy harvesting are less explored in research for reasons of practicality and power generation capability. Table 1 shows a summary of the various human energy harvesting sources and their practicality.

Mechanical energy can be harvested by using motion energy harvesters, which are classified according to the type of transduction involved. Mitcheson *et al.* (2008) classifies motion energy harvesters into two categories of being force driven and inertia driven; Three possible architectures exist for inertia driven harvesters. They are VDRG (Velocity Damped Resonant Generator), CDRG (Coloumb-Damped Resonant Generator); and CFPG (Coulomb Force Parametric Generator). VDRG can be implemented with either electromagnetics and piezo-electrics whereas CDRG and CFPG architectures use electrostatics. Their performance was simulated and evaluated for various excitation schemes and generator scales. Except for MEMS devices with very small excitation in the

order of 0.5mm, it was found that VDRG architecture had the best overall performance considering power density and generator size. Beeby *et al*. (2006) reviewed research conducted on piezoelectric, electromagnetic and electrostatic generators for energy harvesting from vibrations. They describe their practicality depending on the geometry and application, with electromagnetic generators offering better performance and reliability on a macro scale.

TABLE 2.1: Summary of human energy harvesting sources

Source	**Technology**	**Practicality**
Blood Pressure	Generates electricity from pressure fluctuations in the blood, using piezo electrics	Low power generating potential, expensive MEMS technology required
Body Heat	Heat generated by the human body harvested with either thermoelectric effect or a heat engine	Low power generating potential, cumbersome arrangement, low practicality
Breathing	Energy recovery from either respiratory air movement or muscular contractions	Low power generating potential, uncomfortable arrangement
Motion-Positive Actuation	Impact forces on piezo electric materials or compliant mechanism. e.g. Footfalls	Highest power generating potential, may require modifications and complex circuits

Motion-Inertial Actuation	Inertial weights used to scavenge mechanical power from limb motion	High power generating potential, relatively cheaper

The principle of human energy harvesting relies on extracting energy in a non-intrusive and comfortable method. Figure 2.1 shows a high-level representation of the human body and the mode of energy harvesting through limb motion. Several researchers have explored the concept of harvesting energy from every day human activities. Yun *et al*. (2011) experimentally recorded acceleration data for a 24 hour time period for six different body parts and presented the potential of inertial energy harvesters. The experiment showed that the ideal locations would be the ankle, knee and wrist with ±10 G's, ±6 G's and ±6 G's of acceleration respectively. It is evident that human energy harvesting potential from limb motion is the highest when compared to other sources. Some notable approaches in inertial harvesting from human limb motion are mentioned. Rome *et al.* (2005) investigated the feasibility of energy harvesting backpacks while walking with loads. Donelan *et al*. (2008) studied the use of a minimal effort biomechanical generator analogous to regenerative braking. Sato *et al.* (2005) designed a microelectronic device, which can harvest electricity from both thermal and vibrational sources. Pillatsch *et al.* (2013) demonstrated a piezoelectric based inertial harvester worn by a user on the upper arm. Another common approach is the shoe-mounted generator, which integrates a piezoelectric crystal to generate electricity using vibrational impact during walking or running activities. Turri *et al*. (2003) studied human walking dynamics and the applicability of a linear generator to

harvest electricity from the natural walking motion. Xie *et al.* (2009) focused on automatic winding devices and their application in energy harvesting. Green *et al.* (2013) stressed the importance of low frequency harvesters and understanding ambient vibration. Wang *et al.* (2005) developed a prototype improving on the design and power density of two-pole generators used in quartz watches.

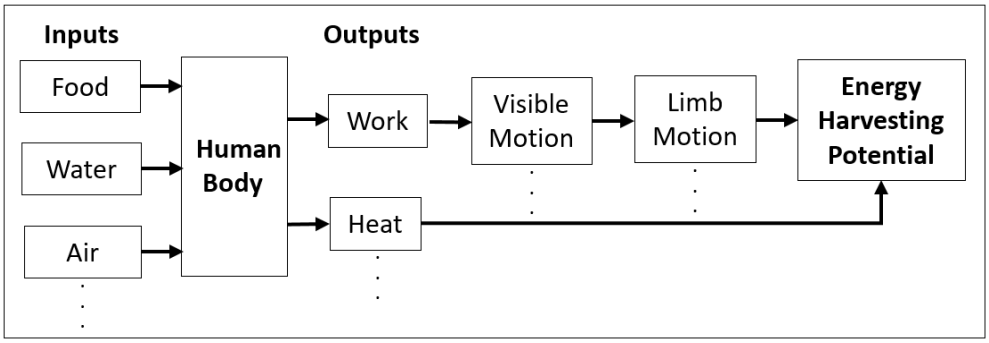

Figure 2.1: High-level representation of human body outputs and available limb motion based energy harvesting

This introduction has outlined some key research work and motivation leading to our approach of a portable wrist-wearable device as a practical and economic solution to human powered energy harvesting. The prototype described here will consist of a pendulum excited by the user's limb movements from everyday activities such as walking or running. The low frequency oscillations are stepped up to high speed rotational motion via a single stage gear train mated to a DC generator, which in turn generates a low frequency alternating current. The output is rectified and filtered with the help of a diode and boost converter circuit to output stable DC power. In the remainder of this chapter starting with Section 2.2, the principle of the auto-winding mechanism explaining the subsystems and a preliminary design of the prototype device is explained. In Section 2.3, a mathematical

model is developed with the dynamics of the human arm-device system to understand the mechanical behavior of the harvester pendulum. The model will serve as a guide to identify optimal design parameters for future research into building a functional harvester prototype. Section 2.4 discusses results for simulated human inputs for two cases of walking and running, to estimate the power generation capability of the device. Finally, Section 2.5 summarizes the chapter with observations and potential future research.

2.2 Design of Harvester Autowinder

The prototype energy harvester is based on the autowinder or automatic watch mechanism commonly used in mechanical watches, which automatically winds the watch spring by harnessing energy from human walking, eliminating the need for manual rewinding. The earliest usage of the mechanism dates to over two centuries ago; however, the mechanism is still used in some mechanical watches in the market. Watch manufacturers like Citizen and Seiko have used this principle to generate electric power for a self-powered, quartz excited timepiece. One of the most commonly used designs in the industry consists of an oscillating pendulum coupled with a gear train to transmit the movement. The rotor has two parts: the support section and weighted section, both of which are riveted. The support section is made of steel to absorb shocks, and the weighted section is made of tungsten. A ball bearing on the oscillating weight reduces the friction. The rotational movements are transmitted to the gear train. The reverser is a key component of this mechanism, which consists of the reversing wheel, the reversing coupling wheel, the auxiliary reversing wheel and the auxiliary reversing coupling wheel. There are four pawls

that convert the bidirectional movement to unidirectional movement of the reversing pinion. The pawls work in a similar fashion to that of a bicycle freewheel.

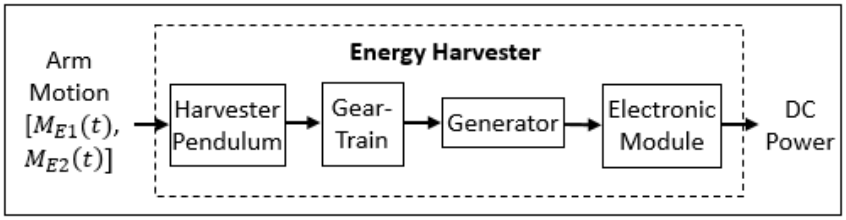

Figure 2.2: Representation of energy flow in the energy harvester

The principle of using an eccentric mass to generate usable electric power can be scaled up to serve as a portable power source for consumer electronics such as smartwatches and smartphones. Figure 2.2 shows the energy flow diagram of the conceptual harvester device through the main subsystems, where human motion is the input. The harvester pendulum is excited from human arm motion, and is mated to the gear train which converts the low frequency oscillations. The stepped up oscillations turn the generator, generating electric power with a varying polarity. Unlike the auto-winder device, the harvester can be designed without a reversing mechanism, since a polarity correction can be achieved using efficient rectifier circuits. The electronic module ensures the electric power generated is conditioned for real world applications. A design layout of the harvester device was created with these main subsystems in consideration. A CAD model render showing the layout of the various components in the exploded view is shown in Figure 2.3. The main subsystems of the harvester device and their purpose are briefly described below.

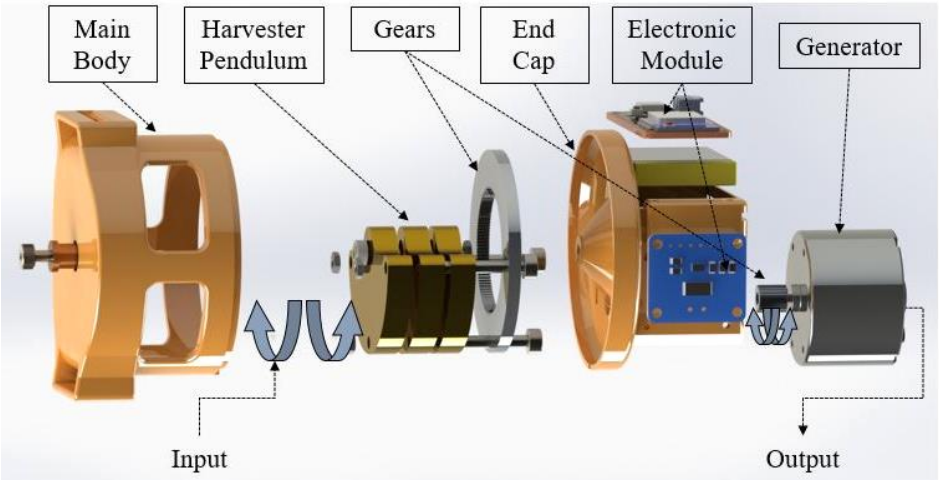

Figure 2.3: Prototype energy harvester device with internal components

Harvester Pendulum: Owing to the high rotational inertia of the coupled gear train and generator system, the harvester pendulum is designed as three semi-circular discs machined from a high density alloy like brass for a high moment of inertia. The pendulum rests on the support shaft with the help of low friction ball bearings, allowing for easy oscillation to small user inputs and is the first step in converting oscillating human motion into rotational motion.

Gear-Train Gears: The frequency of human arm swing is usually in the order of 0.5 to 3 Hz depending on the type of activity. This oscillatory motion is converted into a higher frequency rotational motion to suit the characteristics of the generator with the help of a gear train. With the size constraint and available off-the shelf components, the design aims for a gear ratio of 1:5 for the generator end. The gear train has a planetary layout which enables a compact design. The Pendulum rests on a support shaft and is directly coupled to a 120 teeth ring gear. A 24 teeth planet gear connected to the generator shaft mates with

this ring gear, giving a final gear ratio of 1:5. A sun gear is avoided by directly coupling the planet gear to the generator as seen in Figure 2.3.

Generator: A DC generator may be used to generate electric power from the input motion. The stepped up rotational motion is used to power the DC generator to generate electric power. A brushed DC motor which is economical and commonly available has the desirable characteristics for use as a generator, and is a good choice for the prototype. Since commercially available DC motors have a high rotational speed at the rated voltage, a DC motor with a lower rated speed at higher voltage is selected in order to obtain high output at low input rpm. Constraints on size and weight determines the choice, with a direct dependency on the size and weight of the pendulum as well.

Electronic Module: The oscillatory input from the user arm results in oscillations in the pendulum and consequently the output from the DC generator will be alternating current. The electronic module will consist of subcomponents for rectifying and converting the current to usable DC power. A bridge rectifier based on Schottky diodes may be used for rectification with significantly lower forward voltage losses. To filter out any spikes, an RC circuit is incorporated to smooth out the variable voltage and current. Along with the power conditioning circuits, a data logging system will also be included for experimental validation of the prototype.

Enclosure Assembly: The harvester mechanism is supported in an enclosure assembly consisting of two components; the main body and the end cap. The main body is designed to be a chassis and a protective cover for the pendulum and the gear train, and aligns the support shaft with the end cap. The end cap houses the electronic module consisting of the

rectifier, filtering circuits, the data logging micro controller board and an electric load to measure the power output. Both the components will be 3-D printed using materials such as ABS or PLA to reduce gross weight of the device without compromising on structural rigidity.

2.3 Mathematical Model

The human arm is a complex bio-mechanical system with multiple linkages controlled by several muscle groups to create a coordinated movement in three-dimensional space. To simplify the analysis, the human arm will be considered a forced double pendulum in the X-Y plane with torque being applied at each pivot point (Burdet *et al*., 2000). As shown in Figure 4, the upper arm is considered as the first pendulum link pivoted at the shoulder and the forearm is considered to be the second pendulum link. A pendulum attached to the farthest link with respect to the human body would then represent a third link or pendulum oscillating to the user's inputs. Thus, the combined user-pendulum system can be modeled as a triple pendulum. The system's equations of motion will be derived based on eight assumptions.

A.1: The pendulum system is considered on a sagittal plane coincident with the human arm motion.

A.2: The upper and lower arms are assumed to be cylindrical rods of uniform radii r_1 and r_2, with a mass, length, and inertia of m_1, l_1 *and* I_1 and m_2, l_2 *and* I_2 with mass centers located at e_1 and e_2 respectively.

A.3: The upper and lower arm moment of inertias are $I_1 = 0.25\, m_1 {r_1}^2 + 0.33\, m_1 {l_1}^2$ and $I_2 = 0.25\, m_2 {r_2}^2 + 0.33\, m_2 {l_2}^2$.

A.4: The upper and lower arm mass centers are $e_1 = 0.5\, l_1$ and $e_2 = 0.5\, l_2$.

A.5: The harvester rotor is considered to be a semi-circular disc with a mass, radius and inertia of m_3, l_3, I_3 and mass center at $e_1 = 4.188\, l_3$ and $I_3 = 0.5\, m_3 {l_3}^2$.

A.6: Damping is considered to act at first and second pivot points for the pendula; however, air resistance is neglected.

A.7: User inputs are modeled as time dependent and constant moments, $M_{E1}(t)$ and M_{E2} acting on the first and second pivots respectively.

A.8: The behavior of the mechanical pendulum is simulated, omitting the effect of the DC generator.

The triple pendulum dynamics may be developed using Generalized Lagrangian equations. The mass center coordinates for each pendulum $x_n$and y_n for $(n = 1,2,3)$, are given by

$$x_1 = e_1 \sin\theta_1,\ y_1 = -e_1 \cos\theta_1 \tag{2.1a}$$

$$x_2 = l_1 \sin\theta_1 + e_2 \sin\theta_2, \quad y_2 = -\, l_1 \cos\theta_1 - e_2 \cos\theta_2 \tag{2.1b}$$

$$x_3 = l_1 \sin\theta_1 + l_2 \sin\theta_2 + e_3 \sin\theta_3\ , y_3 = -l_1 \cos\theta_1 - l_2\, cos\, \theta_2 - e_3 \sin\theta_3 \tag{2.1c}$$

where l_n, θ_n, and e_n denote the pendulum lengths, angles, and mass center distances. The first derivatives for the respective coordinates become

$$\dot{x}_1 = -\, e_1 \dot{\theta}_1 \cos\theta_1\ , \dot{y}_1 = e_1\, \dot{\theta}_1\, sin\, \theta_1 \tag{2.2a}$$

$$\dot{x}_2 = l_1 \dot{\theta}_1\, cos\, \theta_1 + e_2 \dot{\theta}_2 \cos\theta_2\ , \dot{y}_2 = l_1 \dot{\theta}_1\, sin\, \theta_1 + \ e_2 \dot{\theta}_2 \sin\theta_2 \tag{2.2b}$$

$$\dot{x}_3 = l_1\dot{\theta}_1 \cos\theta_1 + l_2\dot{\theta}_2 \cos\theta_2 + e_3\,\theta_3 \dot{\cos}\,\theta_3,$$
$$\dot{y}_3 = l_1\dot{\theta}_1 \sin\theta_1 + l_2\dot{\theta}_2 \sin\theta_2 + e_3\,\dot{\theta}_3 \sin\theta_3 \quad (2.2c)$$

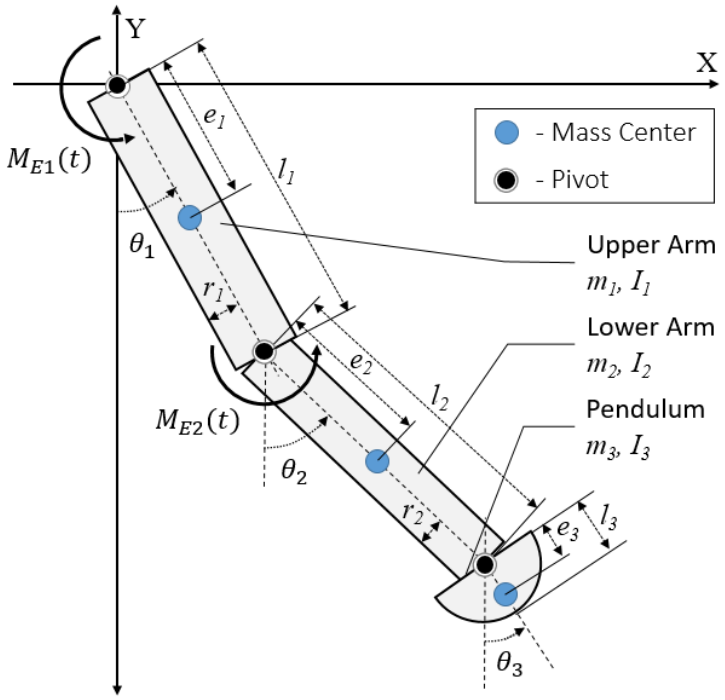

Figure 2.4: Triple pendulum model of human arm and harvester pendulum

The Lagrangian equation for the mechanical system may be stated as

$$\frac{d}{dt}\left(\frac{\partial T}{\partial \dot{q}_n}\right) - \frac{\partial T}{\partial q_n} + \frac{\partial V}{\partial q_n} = Q_n \quad (2.3)$$

where q_n is the n^{th} generalized coordinate and Q_n the n^{th} generalized force. The system potential energy, V, is the sum of contributions of the three link with respect to their mass centers so that

$$V = -(m_1 g e_1 + (m_2 + m_3) g l_1)\cos\,\theta_1 - (m_2 g e_2 + m_3 g l_2)\cos\theta_2 - (m_3 g e_3)\cos\theta_3 \quad (2.4)$$

This expression can be simplified and rewritten as

$$V = -\sum_{n=1}^{3} L_n \cos\theta_n \tag{2.5}$$

where $L_1 = m_1 g e_1 + (m_2 + m_3) g l_1$, $L_2 = m_2 g e_2 + m_3 g l_2$ and $L_3 = m_3 g e_3$.

The kinetic energy of the system, T, is calculated by taking the sum of kinetic energies of each of the links for translational and rotational motion so that

$$T = \frac{1}{2}\sum_{n=1}^{3} m_n(\dot{x}_n^2 + \dot{y}_n^2) + \frac{1}{2}\sum_{n=1}^{3} I_n \dot{\theta}_n^2 \tag{2.6}$$

Substituting and simplifying, the expression may be restated as

$$T = \frac{1}{2}\sum_{n=1}^{3} A_n\, \dot{\theta}_n^2 + \sum_{n=1}^{3}\sum_{j=1}^{2}\left(B_{nj}\dot{\theta}_n\dot{\theta}_j \cos(\theta_n - \theta_j)\right) \tag{2.7}$$

where the grouped term A_n represents $A_1 = I_1 + {e_1}^2 m_1 + {l_1}^2(m_2 + m_3)$, $A_2 = I_2 + {e_2}^2 m_2 + {l_2}^2 m_3$, and $A_3 = I_3 + {e_3}^2 m_3$ for $n = 1,2,3$. Similarly, B_{nj} represents $B_{12} = m_2 e_2 l_1 + m_3 l_1 l_2, B_{13} = m_3 e_3 l_1, B_{23} = m_3 e_3 l_2$ for $n = 1,2,3$ and $j = 1,2$.

The potential and kinetic energy equations (5) and (7) are substituted in the Lagrangian equation (3) to obtain the pendulum dynamics

$$\begin{aligned}\frac{d}{dt}\left(\frac{\partial T}{\partial \dot{\theta}_1}\right) - \frac{\partial T}{\partial \theta_1} + \frac{\partial V}{\partial \theta_1} &= A_1\, \ddot{\theta}_1 + B_{12}\cos(\theta_1 - \theta_2)\ddot{\theta}_2 + B_{13}\cos(\theta_1 - \theta_3)\ddot{\theta}_3 \\ &+ B_{12}\sin(\theta_1 - \theta_2)\dot{\theta}_2^2 + B_{13}\sin(\theta_1 - \theta_3)\dot{\theta}_3^2 + L_1 \sin\theta_1\end{aligned} \tag{2.8a}$$

$$\begin{aligned}\frac{d}{dt}\left(\frac{\partial T}{\partial \dot{\theta}_2}\right) - \frac{\partial T}{\partial \theta_2} + \frac{\partial V}{\partial \theta_2} &= A_2\, \ddot{\theta}_2 + B_{12}\cos(\theta_1 - \theta_2)\ddot{\theta}_1 + B_{23}\cos(\theta_2 - \theta_3)\ddot{\theta}_3 - \\ &B_{23}\sin(\theta_2 - \theta_3)\dot{\theta}_1^2 + B_{23}\sin(\theta_2 - \theta_3)\dot{\theta}_3^2 + L_2 \sin\theta_2\end{aligned} \tag{2.8b}$$

$$\frac{d}{dt}\left(\frac{\partial T}{\partial \dot{\theta}_3}\right) - \frac{\partial T}{\partial \theta_3} + \frac{\partial V}{\partial \theta_3} = A_3\,\ddot{\theta}_3 + B_{12}\cos(\theta_1 - \theta_2)\ddot{\theta}_1 + B_{23}\cos(\theta_2 - \theta_3)\ddot{\theta}_2 - B_{13}\sin(\theta_1 - \theta_3)\dot{\theta}_1^2 - B_{23}\sin(\theta_2 - \theta_3)\dot{\theta}_2^2 + L_3\sin\theta_3 \quad (2.8c)$$

To determine the generalized forces, all the non-conservative forces are considered. This includes the applied moments acting at the upper and lower pendulum joints denoted by $M_{E1}(t)$ and M_{E2}, which will be explained section 4, and the viscous damping acting at each revolute joint. Let $Q_n$be the generalized forces acting on the nth pendulum. Similarly, define c_n as the viscous damping coefficient at each joint. The damping moment acting at a joint due to the relative rotation of one link with respect to the other can be considered as a moment equal in magnitude but opposite in direction in the consecutive link. The generalized forces acting on each pendulum are given by

$$Q_1 = M_{E1}(t) - c_1\dot{\theta}_1 + c_2\left(\dot{\theta}_2 - \dot{\theta}_1\right) \quad (2.9a)$$

$$Q_2 = M_{E2} - c_2\left(\dot{\theta}_2 - \dot{\theta}_1\right) + c_3\left(\dot{\theta}_3 - \dot{\theta}_2\right) \quad (2.9b)$$

$$Q_3 = -c_3\left(\dot{\theta}_3 - \dot{\theta}_2\right) \quad (2.9c)$$

The equations of motion describing the triple pendulum system is obtained by equating equations (8) and (9) and following equation (3) so that

$$A_1\,\ddot{\theta}_1 + B_{12}\cos(\theta_1 - \theta_2)\ddot{\theta}_2 + B_{13}\cos(\theta_1 - \theta_3)\ddot{\theta}_3 + B_{12}\sin(\theta_1 - \theta_2)\dot{\theta}_2^2 + B_{13}\sin(\theta_1 - \theta_3)\dot{\theta}_3^2 + L_1\sin\theta_1 + c_1\dot{\theta}_1 - c_2\left(\dot{\theta}_2 - \dot{\theta}_1\right) = M_{E1}(t) \quad (2.10a)$$

$$A_2\,\ddot{\theta}_2 + B_{12}\cos(\theta_1 - \theta_2)\ddot{\theta}_1 + B_{23}\cos(\theta_2 - \theta_3)\ddot{\theta}_3 - B_{23}\sin(\theta_2 - \theta_3)\dot{\theta}_1^2 + B_{23}\sin(\theta_2 - \theta_3)\dot{\theta}_3^2 + L_2\sin\theta_2 + c_2\left(\dot{\theta}_2 - \dot{\theta}_1\right) - c_3\left(\dot{\theta}_3 - \dot{\theta}_2\right) = M_{E2} \quad (2.10b)$$

$$A_3\,\ddot{\theta}_3 + B_{12}\cos(\theta_1-\theta_2)\ddot{\theta}_1 + B_{23}\cos(\theta_2-\theta_3)\ddot{\theta}_2 - B_{13}\sin(\theta_1-\theta_3)\dot{\theta}_1^2 - B_{23}\sin(\theta_2-\theta_3)\dot{\theta}_2^2 + L_3\sin\theta_3 + c_3\left(\dot{\theta}_3-\dot{\theta}_2\right) = 0 \quad (2.10c)$$

Finally, equations (10) may be expressed in matrix form using the state vector $\boldsymbol{\theta} = [\theta_1 \quad \theta_2 \quad \theta_3]^{\boldsymbol{T}}$ as

$$\boldsymbol{M(\theta)\ddot{\theta} + N(\theta)\dot{\theta}^2 + C\dot{\theta} + p(\theta) = F_E(t)} \quad (2.11)$$

where $M(\theta)$ is the state dependent mass term, $N(\theta)$ is the state dependent non-linearities, C the damping matrix, $p(\theta)$ the potential energy matrix and $F_E(t)$ is the force matrix given by equations (12a) to (12e).

$$\boldsymbol{M(\theta)} = \begin{bmatrix} A_1 & B_{12}\,cos(\theta_1-\theta_2) & B_{13}\,cos(\theta_1-\theta_3) \\ B_{12}\,cos(\theta_1-\theta_2) & A_2 & B_{23}\,cos(\theta_2-\theta_3) \\ B_{13}\,cos(\theta_1-\theta_3) & B_{23}\,cos(\theta_2-\theta_3) & A_3 \end{bmatrix} \quad (2.12a)$$

$$\boldsymbol{N(\theta)} = \begin{bmatrix} 0 & B_{12}\,sin(\theta_1-\theta_2) & B_{13}\,sin(\theta_1-\theta_3) \\ -B_{12}\,sin(\theta_1-\theta_2) & 0 & B_{23}\,sin(\theta_2-\theta_3) \\ -B_{13}\,sin(\theta_1-\theta_3) & -B_{23}\,sin(\theta_2-\theta_3) & 0 \end{bmatrix} \quad (2.12b)$$

$$\boldsymbol{C} = \begin{bmatrix} c_1+c_2 & -c_2 & 0 \\ -c_2 & c_2+c_3 & -c_3 \\ 0 & -c_3 & c_3 \end{bmatrix} \quad (2.12c)$$

$$\boldsymbol{p(\theta)} = [L_1\,sin\,\theta_1 \quad L_2\,sin\,\theta_2 \quad L_3\,sin\,\theta_3]^{\boldsymbol{T}} \quad (2.12d)$$

$$\boldsymbol{F_E(t)} = [M_{E1}(t) \quad M_{E2} \quad 0]^{\boldsymbol{T}} \quad (2.12e)$$

2.4 Case Study

The mathematical model of the triple pendulum is used to simulate common everyday human activities and the response is evaluated. The equations of motion for the triple pendulum system, denoted by equation (11), are simulated in MATLAB with the input denoted by $F_E(t)$. Since $M_{E1}(t)$ and M_{E2} represent the moments acting at the shoulder and

elbow joints, they will vary according to the type of user activity. Two cases are considered – walking and running, for which the input force matrix $F_E(t)$ is derived. The simulation does not take into account the effect of the DC generator on the arm-harvester system, which will be studied in future research. The equation for mechanical power generated by the pendulum P_M can be derived from the torque and angular velocity denoted by τ_M and ω_M given by

$$P_M = \tau_M \omega_M = I_3 \ddot{\theta}_3 \dot{\theta}_3 \tag{2.13}$$

where $I_3 = 0.5\, m_3 {l_3}^2$. The power generated is proportional to the inertia of the pendulum and the angular acceleration and velocities imparted on it by human input. The power output from the energy harvester is analyzed for simulated arm swing motions associated with human walking and running activities. The mass and length for the upper and lower arms are obtained by taking average values from anthropometric database available (David A.W., 2009). The pendulum is assumed to be a semi-circular disc of dimensions and mass acceptable for portable use.

2.4.1 Walking (Case 1)

Walking is one of the most common activities a typical individual engages in on a typical day. Several muscle groups are responsible for the smooth periodical actuation of the arms. The reason behind human arm swing while walking is an interesting research topic which has been explored with varying conclusions such as minimizing energy expenditure, (Ortega *et al*., 2008; Umberger, 2008), counteracting angular momentum by the lower body (Bruijn *et al*. 2008; Herr and Popovic, 2008) and adding stability (Jackson *et al*., 1983, Ortega *et al*., 2008). Nevertheless, human arm swing parameters have been

experimentally measured to indicate significant torques in the shoulder in the order of 8 to 12 Nm; (Elftman, 1939, Collins *et al.*, 2009) suggesting that human arm swinging is a continuously forced actuation rather than a reactive response to body displacements and moments.

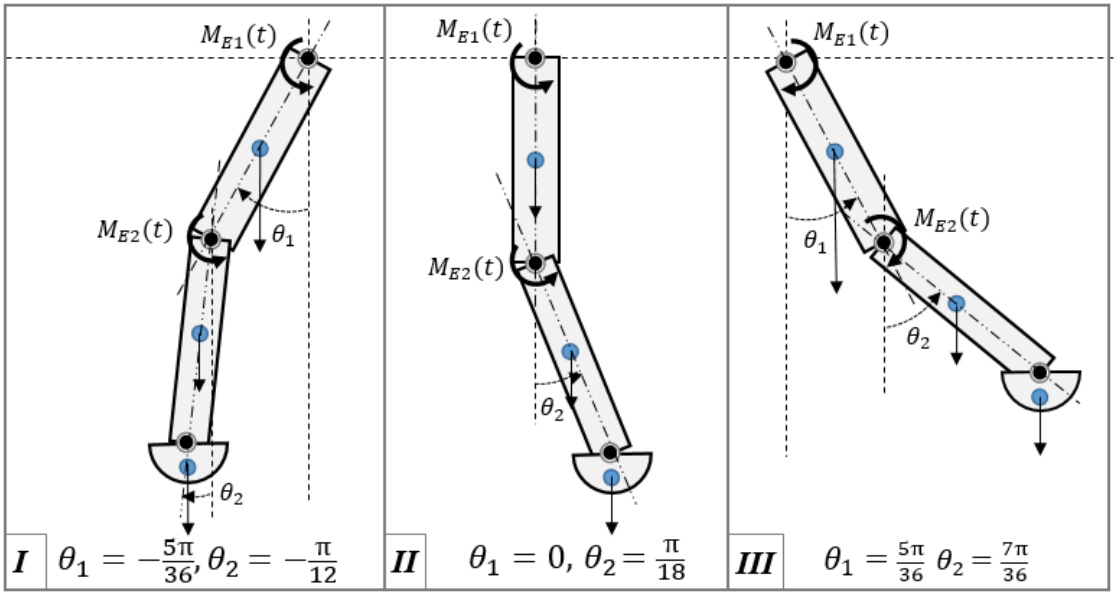

Figure 2.5: Sequence of arm motion in the walking scenario (Case 1) from position I to III

The torque generated and the cadence of actuation by the upper and lower arm muscles can vary widely from person to person, and hence a simplified arm swing is simulated using approximated torque functions that imitate human arm swing behavior during walking. As explained in the mathematical model, $M_{E1}(t)$ and $M_{E2}(t)$ represent the moments acting on the upper and lower arm pivot points. A simplified human arm swing cycle shown in three steps is shown in Figure 2.5. To imitate this target motion, assume that

$$M_{E1}(t) = q_{1w}\, sin(2\pi f_w t), \tag{2.14a}$$

$$q_{1w} = (m_1 e_1 \sin(25^o) + m_2 l_1 \sin(25^o) + m_2 e_2 \sin(10^o + 25^o) + m_3 l_1 \sin(25^o) + m_3 l_1 \sin(25^o) + m_3 l_2 \sin(10^o + 25^o))g \tag{2.14b}$$

and

$$M_{E2} = q_{2w}, \tag{2.14c}$$

$$q_{2w} = (m_2 e_2 + m_3 l_2) \sin(10^o + 25^o)\, g \tag{2.14d}$$

where q_{1w} and q_{2w} are the maximum torques applied by the upper and lower arm muscles to assume the target walking positions, found out by taking moments at the respective pivots. The frequency of arm swing for walking is assumed to be $f_w = 0.7\ Hz$, to imitate a normal walking pace.

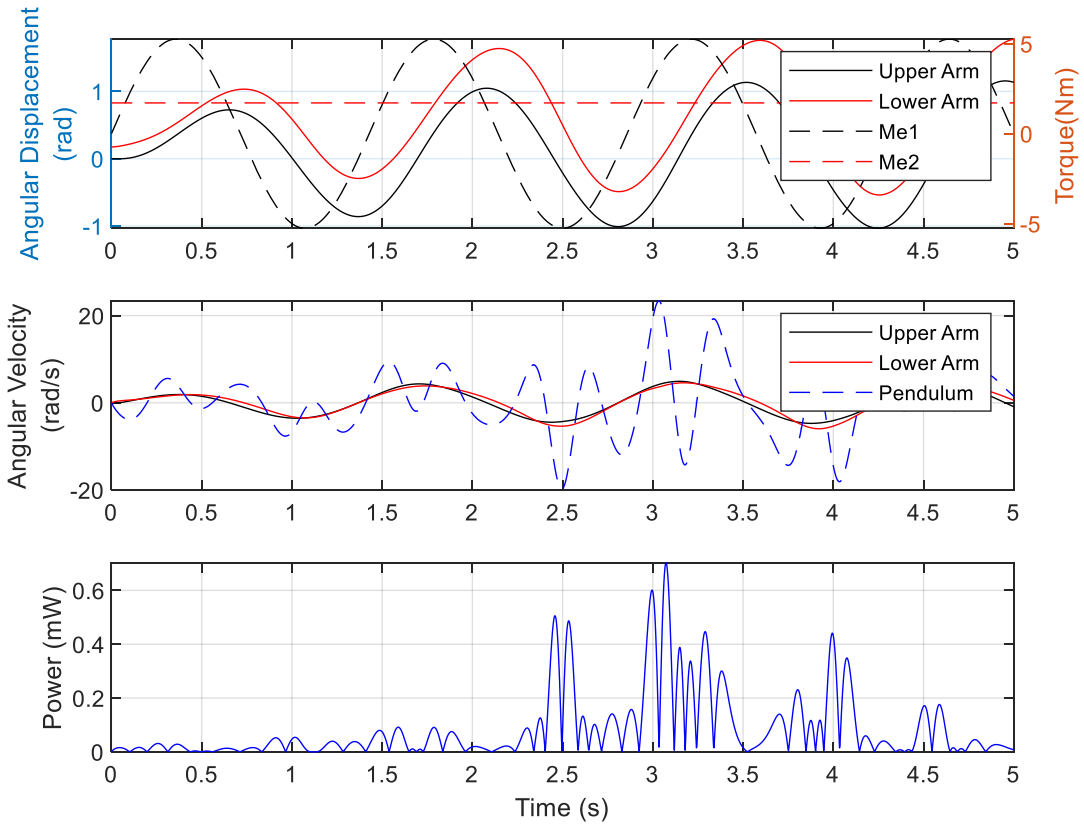

Figure 2.6: For walking (Case 1): (a) Human input moments and angular displacement, (b) Angular velocities of each pendulum, and (c) Power generation available from harvester pendulum.

The parameter values assumed for this case study are given in Table 2.3. A majority of the driving torque is provided by the upper arm while the lower arm provides a sustaining torque of a lower magnitude. A viscous damping coefficient of 1 Nms is assumed at the upper and lower arm joints to simulate the muscular damping behavior. The initial angles for the upper arm, lower arm and the pendulum are assumed to be as shown in position II in Figure 5. The simplified walking arm swing is simulated for a runtime of 5 seconds using MATLAB. Figure 2.6(a) shows the angular displacements of the upper arm, lower arm,

and the pendulum versus the input moments into the system. Both arms exhibit near-sinusoidal angular displacements, closely imitating walking motion. The angular velocities of the pendula are shown in Figure 2.6(b), where it can be seen that the angular acceleration of the pendulum is significantly higher than that of the upper and lower arms, showing torque availability for energy harvesting. With Eq. (11), the instantaneous power output in milli-Watts from the harvester is obtained as shown in Figure 2.6(c). The peak power output obtained was 0.7 mW whereas the energy harvested over the time of 5 seconds was 0.42 mJ.

Table 2.2**:** Summary of Parameter Values for Case Studies

Parameter	**Value**	**Units**	**Parameter**	**Value**	**Units**
c_1	1.0	N m s	l_3	0.025	m
c_2	1.0	N m s	m_1	2.6	kg
c_3	0	N m s	m_2	1.6	kg
e_1	0.12	m	m_3	0.18	kg
e_2	0.125	m	q_{1r}	6.247	Nm
e_3	0.0212	m	q_{2r}	2.979	Nm
f_r	2	Hz	q_{1w}	5.256	Nm
f_w	0.7	Hz	q_{2w}	1.709	Nm
g	9.81	m s^{-2}	r_1	0.05	m
l_1	0.24	m	r_2	0.035	m
l_2	0.25	m			

2.4.2 Running (Case 2)

The average human expends a considerable amount of power, often above 600 Watts for a running speed of 5 kph. This means a greater potential for energy harvesting compared to walking, owing to the higher magnitude and frequency of the sinusoidal moments acting at the upper and lower arm joints. Again, a simplified arm cycle for running is considered as shown in Figure 2.7. Unlike walking, a 90^o angular displacement between the upper and the lower arm is assumed throughout the running scenario, with positon II showing the initial angles. Since the holding torques at the joints in Steps I and III are unequal, the sinusoidal moment is modelled differently compared to the walking sequence. Considering the upper arm, the torque at maximum actuation angle of 25^o shown in Step III should be the highest since the lever arm for the lower arm and harvester is larger, contributing to increased moment.

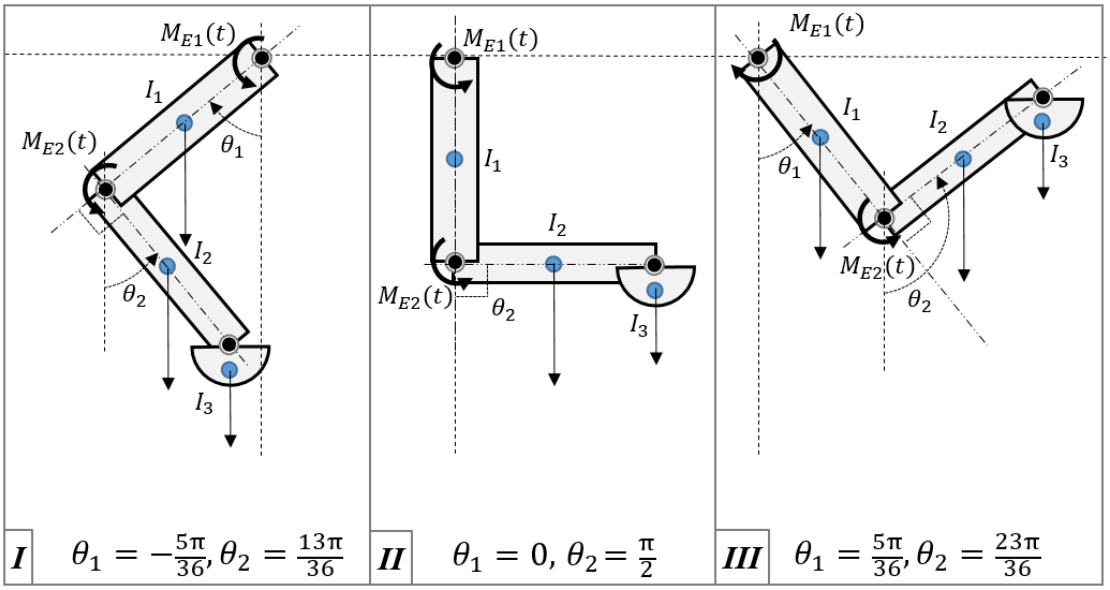

Figure 2.7: Sequence of arm motion in the running scenario (Case 2) from position I to III

To simulate arm swing during running, assume

$$M_{E1}(t) = q_{1r}\, sin(2\pi f_r t), \tag{2.15a}$$

$$q_{1r} = (m_1 e_1 \sin(25^o) + m_2 l_1 \sin(25^o) + m_2 e_2 \sin(90^o + 25^o) + m_3 l_1 \sin(25^o) + m_3 l_1 \sin(25^o) + m_3 l_2 \sin(90^o + 25^o))g \tag{2.15b}$$

and

$$M_{E2} = q_{2r}, \tag{2.15c}$$

$$q_{2r} = (m_2 e_2 + m_3 l_2)g \tag{2.15d}$$

where q_{1r} and $q_{2r}$are the maximum torques acting at the upper and lower arm joints with a frequency of $f_r = 2\, Hz$ assumed for the driving torque at the upper arm to simulate a running pace. The viscous damping coefficient values are assumed to be the same as in the case of walking. Table 2.3 gives the parameter values assumed for this case. The running sequence is simulated for a run time of 5 seconds. Figure 2.8(a) shows the response of the upper and lower arms to input moments $M_{E1}(t)$ and M_{E2}. Figures 2.8(b) and (c) show the angular velocities of the pendula over time. The peak power output obtained was around 1.8 mW, with an energy output of 2.06 mJ over a period of 5 seconds. With the simulated human running having a higher torque magnitude and frequency, the energy generated is more than double than that of walking. It should be noted that a higher frequency of actuation need not coincide with higher power output, since the difference between the

natural oscillating frequency of the pendulum and the simulated actuation frequency of the arms would play a crucial role in the excitation behavior of the pendulum.

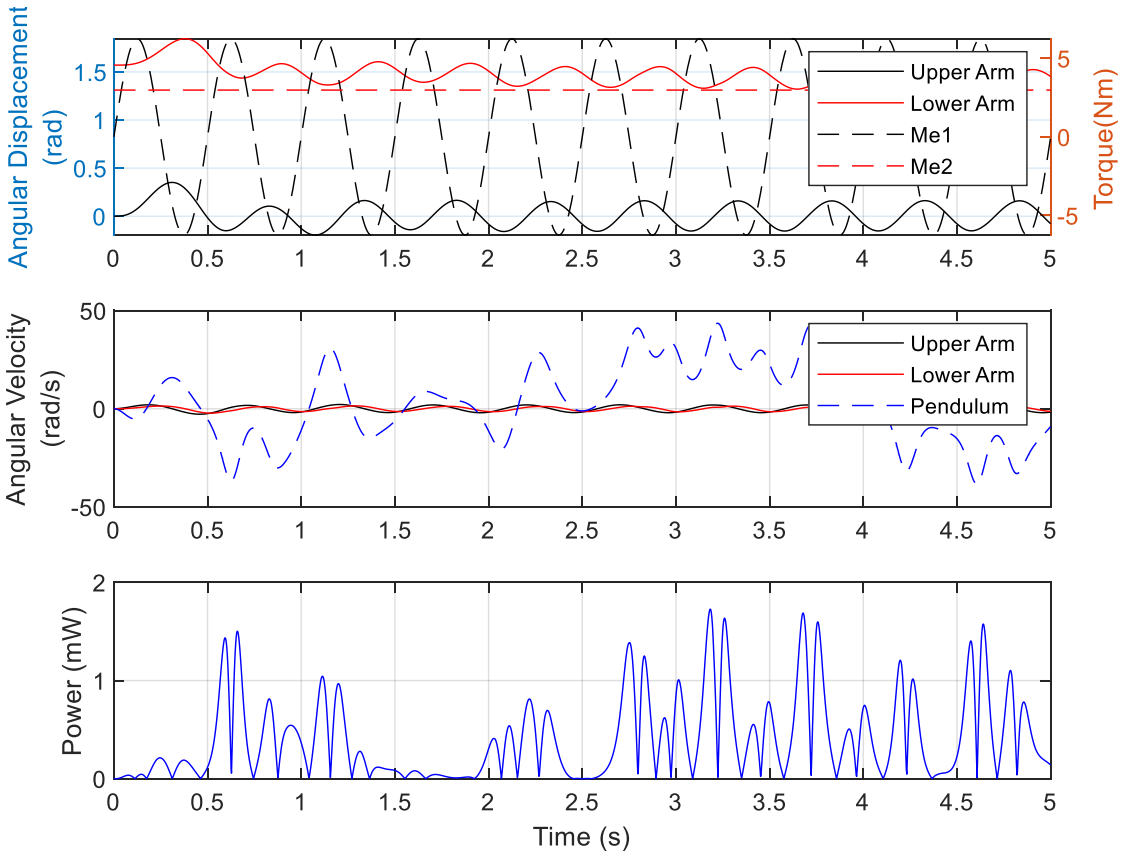

Figure 2.8: For running (Case 2): (a) Human input moments, (b) Angular velocities of the pendula, and (c) Power generation available from harvester pendulum.

2.5 Summary

A mobile energy harvesting device capable of generating power from daily life human activities has been investigated. The equations of motion of the user-device system was derived based on a triple pendulum system using the Lagrangian approach. The human arm swing during the activities of walking and running were simulated using approximated sinusoidal functions as the moment inputs at the upper and lower arm joints to resemble

walking motion. For a period of 5 seconds, the energy generated during walking was 0.42 mJ while running generated 2.06 mJ of energy. It should be noted that the triple pendulum exhibits a highly chaotic response to inputs, and thereby minute changes in damping or excitation frequency will output widely varying results. The damping assumed at the upper and lower arm joints are tuned to resemble walking and running motions with the input torques, which may not simulate actual damping values for the human arm. The efficacy of the device as an offline renewable power source can be increased by storing the intermittent energy from the generator into a battery by using appropriate circuitry. In future research, a prototype device will be built to validate the results experimentally for different human activities. The mathematical model will be utilized to understand the expected power output for each activity, providing with important design considerations. Considering a physically active user, such a device has practical consumer applications such as charging cell phones or other portable multi-media devices without depending on the grid, or in military applications where energy harvesting can provide valuable electric power for critical communication devices, offering a great range of flexibility to the user.

CHAPTER THREE

A MOBILE ENERGY HARVESTING AUTOWINDER – BUILD AND TEST

This chapter explains the numerical and experimental studies conducted on the harvester. A mathematical model based on the triple pendulum system was developed to simulate arm motion dynamics and study the electromechanical behavior of the harvester. A prototype harvester was built and tested and validated the predictions from the numerical study.

3.1 Background

In recent years, the need for energy efficient products has increased in multiple sectors including automobiles, consumer appliances, and in the booming market of smartphones. Advances in microprocessor manufacturing and battery technologies strive towards increasing the battery life of such portable devices. However, the developments occurring in these fields do not meet the increasing power demand of digital processors with giga-hertz level computing power. In many cases, a one day-battery life for a mobile device is insufficient to service the needs of heavy usage consumers. This can be especially challenging if there is limited access to the power grid. Portable battery packs are a common method of recharging smartphones on the go, but ultimately the need to charge these devices require additional effort from the user and dependence on the grid. Technologies such as solar and wind energy systems exist but are not portable and rely on external conditions such as time of day, weather, etc. In this regard, harvesting human motion provides several advantages such as increased control and portability for the user.

Harvesting human energy from humans in a non-intrusive way is a plausible renewable energy method. In a time where one third of the world's population owns a smartphone, a self-sustaining portable energy source can offer the user with flexibility and grid independence. Starner (1996) explored how the human body may empower energy harvesting and concluded that impact and inertial methods have the most potential. Jansen *et al.* (2006) proposed several product designs to improve environmental performance of portable electronic devices. Turri *et al.* (2004) considered hip-motion as an excitation source for a linear electro-mechanical generator. Meninger *et al.* (2001) developed a variable capacitor based MEMS system to convert vibrational energy into electrical energy. Finally, Poulin *et al.* (2004) presented a comparative analysis of electromagnetic and piezoelectric systems, concluding that the former has more potential on a macro scale.

The principle of using an eccentric mass to recover energy from human walking has been applied for over two centuries in mechanical watches to wind their main springs. An excellent collection of historic self-winding watches are presented by Breguet *et al.* (2015). Research on scaling up such mechanisms for harvesting human motion can be found in literature. Pillatsch *et al.* (2013) demonstrated a wearable inertial energy harvester based on piezo-electric technology. Xie *et al.* (2009) focused on automatic winding devices and their application in energy harvesting, to generate electric power. Saha *et al.* (2008) explored a mobile energy harvester based on an inertial mass coupled to a magnetic spring. Wang *et al.* (2005) developed a prototype improving on the design and power density of two-pole generators used in quartz watches. Some modern watches operating on battery power utilize the same principle to generate and store power, requiring no battery change

and extending life. A common design by Seiko in their mechanical watches uses an oscillating mass coupled to a gear train through a reversing mechanism. The mechanical system consists of a pawl lever pivoted to an eccentric shaft mated to an intermediate wheel, which winds the coil spring when the pendulum is excited. The pawl lever converts the bidirectional movement to unidirectional movement in a similar fashion to that of a bicycle freewheel.

The principle of inertial energy harvesting is utilized to design and fabricate a robust device which can serve as a portable power solution for electronic devices. The proposed energy harvester features an electrical system with electronics module to condition the DC generator power output rather than a mechanical reversing mechanism (Fry *et al.* 1997; Hama *et al.* 2002). A high-level diagram illustrating the energy harvester appears in Figure 3.1. The rotary pendulum mechanical system is excited by human motion with the planetary gear amplifying the rotational output. The generator in the electrical system converts the rotational shaft motion into DC power. The remainder of this chapter is organized as follows: Section 3.2 explains the harvester design in terms of the mechanical and electrical systems plus the enclosure. Section 3.3 introduces a nonlinear mathematical model of the energy harvester. Representative numerical and experimental results are presented as discussed in Section 3.4. Finally, the chapter is summarized in Section 3.5.

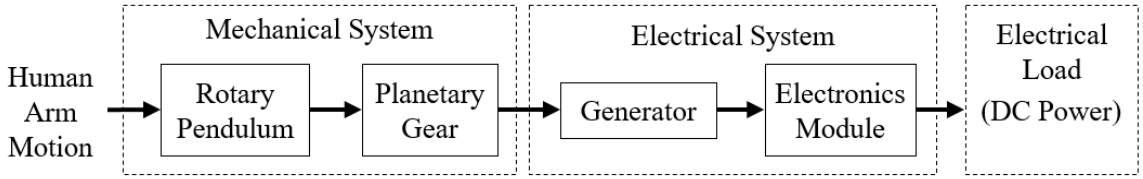

Figure 3.1: High-level diagram of a sustainable energy harvester from the input human motion to the output electrical power

3.2 Design of Energy Harvesting Autowinder

The development of a wearable electro-mechanical energy harvester requires careful component integration and packaging of the system components with attention focused on functionality, size and weight. A set of initial constraints to guide the design process included a volume and gross weight limit of 60x60x60 mm^3, and 200 grams. As shown in Figure 3.2, the harvester's mechanical system of the harvester consists of a rotary pendulum and a planetary gear system. The electrical system features a brushed DC generator and an electronic module comprising of various filtering elements per Figure 3.3. The detailed design requirements for each system components will be explained further in the following sections.

3.2.1 Mechanical System

The mechanical system transfers the kinetic energy of arm motion as illustrated in Figure 3.2. The rotational displacement of the mechanical pendulum is converted to a higher speed with the help of an attached planetary gear-train.

Rotary Pendulum: The principle of inertial harvesting relies on using an eccentric mass's moment of inertia as an excitation source for the power generation system. To maximize energy generation capacity, the pendulum mass should be maximized within

admissible limits. Brass alloy, having a relatively higher density among common machinable alloys, was selected to minimize the relative pendulum volume. A semi-circular profile was chosen for the pendulum to maximize torque input. To aid in experimental investigation, the pendulum is comprised of three identical semi-circular discs fastened with bolts instead of a single machined block. Holes are drilled at the center and towards the disc edge to fit low friction stainless steel ball bearings for shaft mounting and fastening with the ring gear. The pendulum disc has a radius of 25 mm and a combined weight of 180 grams when assembled. The semi-circular disc moment of inertia becomes $I = 0.5\, mr^2$ where m is the pendulum mass and r is the semi-circle radius. The effective system inertia of rotation includes the pendulum, planetary gear, and coupled DC generator.

Planetary Gear: The supplied human motion inputs to the pendulum will be typically of lower frequency and need to be converted to a higher rotational frequency to generate maximum DC power. A planetary gear system is chosen to deliver a 1:5 ratio while offering a compact design. Specifically, the aluminum-2024 ring gear has 120 teeth, planet gear of 24 teeth, and sun gear of 72 teeth, with a diametral pitch of 96 teeth per inch. The ring and planet gears were the input and output, respectively. With stable mounting of the planet gear on the generator shaft, the sun gear that acted as an idler gear was removed from the assembly to reduce weight and minimize gear friction losses. The ring gear maybe attached to the pendulum discs with three bolts, while the planet gear was attached to the DC generator with setscrews. The DC generator was supported by the end cap structure. The support shaft was fixed at both ends, supported by the end cap and the main body.

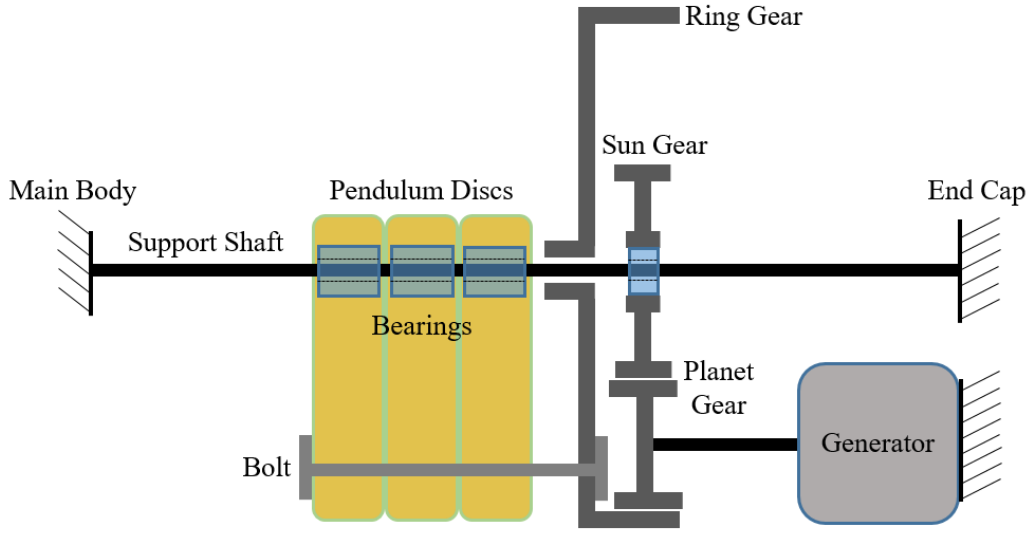

Figure 3.2: Energy harvester mechanical system configuration featuring a rotary pendulum and a planetary gear system

3.2.2 Electrical System

The DC generator was the primary component in the electrical system to convert mechanical motion into electrical power. A bridge rectifier and boost converter prepare the generator's output into a range suitable for powering portable electronic devices. The energy flow through the various system components are displayed in Figure 3.3.

Generator: Brushed DC motors have the characteristic of functioning as a generator when the rotor shaft is subject to input rotation. For this application, the generator for the application should have a low rotor inertia and a high power output from low frequency rotational input. A Hsinen model 330A industrial brushed DC motor with a rated rpm of 1780 at 12V was selected as the generator. The electric machine was directly coupled to the ring gear and thereby the pendulum with the shaft mounted planet gear configuration.

Electronics Module: Human activities such as walking and running exhibit varying pace and cadence depending on the individual. The arm swing motion from the user causes the pendulum to oscillate, which is stepped up through the planetary gear-train and supplied to the DC generator. The resulting inconsistent and alternating current output from the generator must be conditioned before using electronic load devices. which is unsuitable for real world use. In the electronics module, a bridge rectifier is used to rectify the polarity of the output from the generator, while Schottky diodes are used to minimize forward voltage losses (Callaway, 2003). Portable consumer devices such as smartphones and battery packs are charged with a 5V power supply. Since the mechanical input to the pendulum varies, the rectified output is of a variable voltage ranging from 0 to 11.6 V, assuming forward voltage losses of 0.4 V. A boost converter circuit based on the switched mode power supply topology is used to supply constant voltage of 5 volts. The circuit consists of an inductor, capacitor, diode, transistor and an input monitoring IC unit which actively switches the transistor.

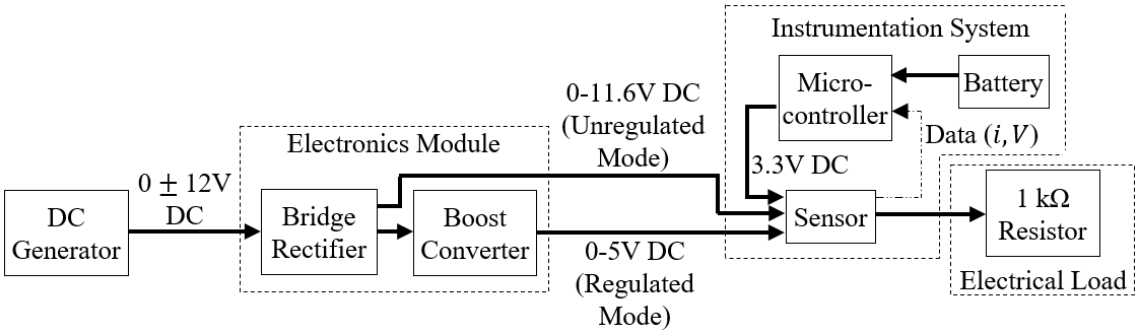

Figure 3.3: Energy harvester electrical system containing the generator, electronics module, instrumentation system, and electrical load for concept validation

3.2.3 Instrumentation System

The energy harvester output data maybe logged using the instrumentation system which consists of a sensor and a microcontroller powered by the onboard battery. A Texas Instruments INA-219 bi-directional current/power monitoring module senses the voltage, current and the real-time power consumed by the load. The sensor communicates the data to a microcontroller over the I2C interface. For untethered testing, an ATmega32u4 8-bit microprocessor equipped with a Wi-Fi chipset is used for streaming this data wirelessly. An onboard battery supplies power to the microcontroller which powers the sensor.

3.2.4 Electrical Load

The experimental validation of the energy harvester requires the introduction of an electrical load. The electrical system in Figure 3.2 supplies electricity to the electrical load which may be a portable electronic device or a representative 1 kΩ resistor. The 1 kΩ resistance serves as the electric load and was used for testing. This resistance ensures an electric load with approximately linear characteristics. Another configuration as shown in Figure 3.4 enables recharging an onboard battery with a voltage regulator in the charging module. A user can then charge a consumer electronic device.

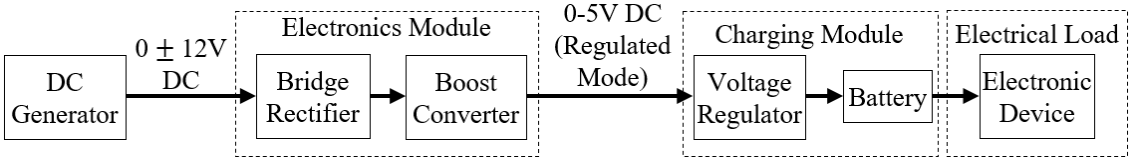

Figure 3.4: Electrical system with attached voltage regulator and rechargeable battery in the charging module to host a portable consumer device electrical load

3.2.5 Three Dimensional Printed Enclosure

The polymer enclosure offers a compact size protective covering for the harvester components and the main support structure for the mechanical system. The enclosure assembly features two parts: the main body that houses the pendulum and the gear-train; and the end cap which integrates the DC generator and the electronic module. Owing to user comfort, the enclosure was designed with an ergonomic form factor and wide fastening straps. For experimental validation and ease of assembly, a single bolt design was implemented. To manufacture the end cap and the main body, 3D printing was used to manufacture the end cap and the main body using bio-friendly PLA material. The prototype harvester with the internal mechanical and electrical systems, shown in Figure 3.5 was pursued, meeting the initial dimensional and weight constraints, allowing it to be worn like a wristwatch.

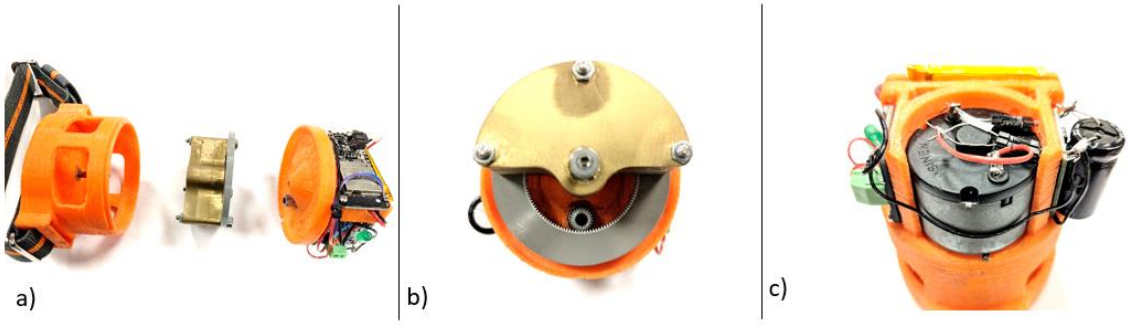

Figure 3.5: Photographs of the prototype energy harvester - (a) Disassembled system showing the main body, mechanical system, and end cap with electrical system, (b) Planetary gear train with accompanying rotary pendulum, and (c) End cap with integrated DC generator, electronics module, and instrumentation system

3.3 Mathematical Model

The swinging motion of the human arm for walking or running can be generally modelled as a double pendulum system in the sagittal plane. As shown in Figure 3.6, the combined arm-harvester may be described as a triple pendulum system subject to two sinusoidal moments acting about the upper and lower arm joints due to muscular actions. To simplify the mathematical analysis, five assumptions will be imposed as follows:

A.1: The human arm and attached harvester is modelled as a triple pendulum system with the upper and lower arms considered to be the first and second pendula.

A.2: The arms are assumed to be uniform cylinders of lengths $l_1$and l_2, radii r_1 and r_2, and masses $m_1$and m_2. The mass centers are situated at $e_1 = 0.5\, l_1$ and $e_2 = 0.5\, l_2$ from their respective pivots. Similarly, the inertias are $I_1 = (m_1 {r_1}^2)/4 + \left(m_1 {l_1}^2\right)/3$ and $I_2 = (m_1 {r_2}^2)/4 + \left(m_1 {l_2}^2\right)/3$.

A.3: The harvester is considered to be the third pendulum connected to a planetary gear-train and DC generator.

A.4: The harvester pendulum uses semi-circular discs pivoted at the center with a radius of l_3, mass m_3, mass center located at $e_3 = \frac{4}{3\pi}\, l_3$, and inertia of $I_3 = 0.5\, m_3 {l_3}^2$ for space consideration.

A.5: The generator is considered to be a DC machine with no frictional losses; the electronics module has no significant electrical resistance.

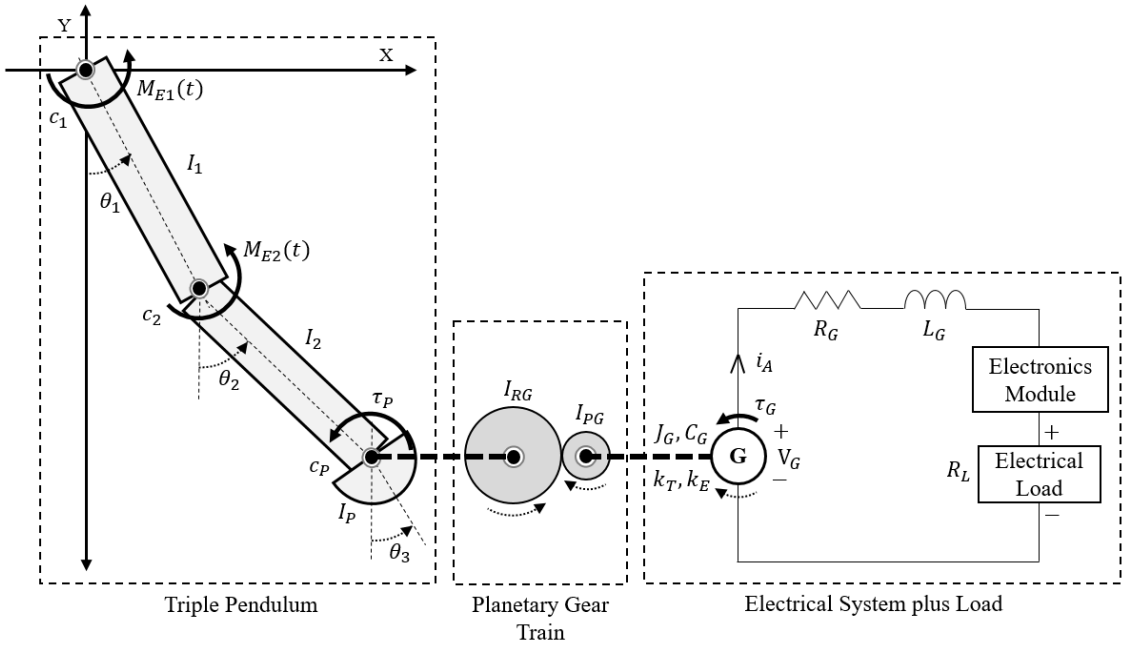

Figure 3.6: Triple pendulum model of the human arm swing, I_1 and I_2, coupled to the harvester system, I_3, with planetary gear train, I_{RG} and I_{PG}, plus the generator, J_G

To derive the governing dynamics let θ_1, θ_2 and θ_3 define the upper arm, lower arm, and harvester pendulum rotational angles. The triple pendulum's equations of motion with torques applied at the upper and lower arm joints, $M_{E1}(t)$ and $M_{E2}(t)$, become

$$A_1\,\ddot{\theta}_1 + B_{12}\cos(\theta_1-\theta_2)\ddot{\theta}_2 + B_{13}\cos(\theta_1-\theta_3)\ddot{\theta}_3 + B_{12}\sin(\theta_1-\theta_2)\dot{\theta}_2^2 + B_{13}\sin(\theta_1-\theta_3)\dot{\theta}_3^2 + U_1\sin\theta_1 + c_1\dot{\theta}_1 - c_2\left(\dot{\theta}_2-\dot{\theta}_1\right) = M_{E1}(t) \quad (3.1)$$

$$A_2\,\ddot{\theta}_2 + B_{12}\cos(\theta_1-\theta_2)\ddot{\theta}_1 + B_{23}\cos(\theta_2-\theta_3)\ddot{\theta}_3 - B_{23}\sin(\theta_2-\theta_3)\dot{\theta}_1^2 + B_{23}\sin(\theta_2-\theta_3)\dot{\theta}_3^2 + U_2\sin\theta_2 + c_2\left(\dot{\theta}_2-\dot{\theta}_1\right) - c_3\left(\dot{\theta}_3-\dot{\theta}_2\right) = M_{E2}(t) \quad (3.2)$$

$$A_3\,\ddot{\theta}_3 + B_{12}\cos(\theta_1-\theta_2)\ddot{\theta}_1 + B_{23}\cos(\theta_2-\theta_3)\ddot{\theta}_2 - B_{13}\sin(\theta_1-\theta_3)\dot{\theta}_1^2 - B_{23}\sin(\theta_2-\theta_3)\dot{\theta}_2^2 + U_3\sin\theta_3 + c_3\left(\dot{\theta}_3-\dot{\theta}_2\right) = 0 \quad (3.3)$$

where $A_1 = I_1 + {e_1}^2 m_1 + {l_1}^2(m_2+m_3)$, $A_2 = I_2 + {e_2}^2 m_2 + {l_2}^2 m_3$, $A_3 = I_3 + {e_3}^2 m_3$, $B_{12} = m_2 e_2 l_1 + m_3 l_1 l_2, B_{13} = m_3 e_3 l_1,$ and $B_{23} = m_3 e_3 l_2$ represent the inertial components, and $U_1 = m_1 g e_1 + (m_2+m_3) g l_1, U_2 = m_2 g e_2 + m_3 g l_2,$ and $U_3 = m_3 g e_3$ represent the potential energy components.

The electro-mechanical characteristics of the DC generator are coupled into these pendulum dynamics. The generator is connected to the rotary pendulum through the planetary gear train. The effective inertia of the pendulum, I_3, thus becomes

$$I_3 = I_P + I_{RG} + (N_{RG}/N_{PG})^2(I_{PG} + J_G) \quad (3.4)$$

where I_P, I_{RG}, I_{PG}, and J_G are the moment of inertias of the pendulum, ring gear, planet gear and the generator, respectively. The terms N_{RG} and N_{PG} denote the ring and planet gear number of teeth, respectively.

Similarly, the effective pendulum damping c_3 can be expressed as

$$c_3 = c_P + (N_{RG}/N_{PG})^2 C_G \quad (3.5)$$

where c_P is the pendulum joint damping and C_G is the generator viscous damping.

To model the DC generator's electrical characteristics, consider the generator torque, τ_G, to be directly proportional to the armature current, i_A, or $\tau_G = k_T i_A = k_T \dot{q}$ where k_T is the motor torque constant. Note that $i_A = \dot{q}$ and $\frac{di_A}{dt} = \ddot{q}$, where q is the electrical charge. The generator torque transferred through the gear train acts as a damping torque τ_P on the pendulum, so that

$$\tau_P = (N_{PG}/N_{RG})k_T\dot{q} \tag{3.6}$$

The summation of the potential differences in the electrical system loop of Figure 6 may be expressed using Kirchhoff's voltage law as

$$L_G\ddot{q} + R_G\dot{q} + R_L\dot{q} + (N_{RG}/N_{PG})k_E\,\dot{\theta}_3 = 0 \tag{3.7}$$

This expression contains the armature inductance, L_G, and armature resistance, R_G, load resistance, R_L, as well as the generator back-emf constant, k_E. The total resistance, R_T, is a sum of the armature and load resistance, or $R_T = R_G + R_L$.

Substituting equations (4) through (7) into equations (1) to (3) results in the state space model with the corresponding state vector $\boldsymbol{\theta} = [\theta_1, \quad \theta_2, \quad \theta_3, \quad q]^{\boldsymbol{T}}$ written as

$$\boldsymbol{M(\theta)\ddot{\theta} + N(\theta)\dot{\theta}^2 + C\dot{\theta} + p(\theta) = F_E(t)} \tag{3.8}$$

In this notation, $\boldsymbol{M(\theta)}$ is the state dependent mass term, $\boldsymbol{N(\theta)}$ is the state dependent non-linearities, $\boldsymbol{C}$ is the damping matrix, $\boldsymbol{p(\theta)}$ is the potential energy matrix and $\boldsymbol{F_E(t)}$ is the excitation matrix.

$$\boldsymbol{M(\theta)} = \begin{bmatrix} A_1 & B_{12}\,cos(\theta_1-\theta_2) & B_{13}\,cos(\theta_1-\theta_3) & 0 \\ B_{12}\,cos(\theta_1-\theta_2) & A_2 & B_{23}\,cos(\theta_2-\theta_3) & 0 \\ B_{13}\,cos(\theta_1-\theta_3) & B_{23}\,cos(\theta_2-\theta_3) & A_3 & 0 \\ 0 & 0 & 0 & L_G \end{bmatrix} \tag{3.9a}$$

$$\boldsymbol{N(\theta)} = \begin{bmatrix} 0 & B_{12}\,sin(\theta_1-\theta_2) & B_{13}\,sin(\theta_1-\theta_3) & 0 \\ -B_{12}\,sin(\theta_1-\theta_2) & 0 & B_{23}\,sin(\theta_2-\theta_3) & 0 \\ -B_{13}\,sin(\theta_1-\theta_3) & -B_{23}\,sin(\theta_2-\theta_3) & 0 & 0 \\ 0 & 0 & 0 & 0 \end{bmatrix} \tag{3.9b}$$

$$\boldsymbol{C} = \begin{bmatrix} c_1 + c_2 & -c_2 & 0 & 0 \\ -c_2 & c_2 + c_3 & -c_3 & 0 \\ 0 & -c_3 & c_3 & -(N_{PG}/N_{RG})\, k_T \\ 0 & 0 & (N_{RG}/N_{PG})\, k_E & R_T \end{bmatrix} \tag{3.9c}$$

$$\boldsymbol{p}(\boldsymbol{\theta}) = [U_1 \sin\theta_1 \quad U_2 \sin\theta_2 \quad U_3 \sin\theta_3 \quad 0]^T \tag{3.9d}$$

$$\boldsymbol{F_E}(\boldsymbol{t}) = [M_{E1}(t) \quad M_{E2}(t) \quad 0 \quad 0]^{\boldsymbol{T}} \tag{3.9e}$$

3.4.0 Numerical and Experimental Results

The coupled mathematical models of the mechanical and electrical behavior of the harvester allow the system's dynamic behavior to be evaluated for different operating scenarios. The system parameters and inputs were identified to emulate human arm motion for both walking and running. The numerical model and overall concept will be validated using the harvester prototype in a real world scenario.

3.4.1 Simulation Results

To investigate the energy harvester's response to human motion, it is important to understand the nature of torques involved in human arm swinging. Research suggests that arm motion is an active response to counteract the generated moments from the various reaction forces involved during human locomotion (Bruijn et al., 2008; Herr and Popovic, 2008). Previously, two case studies were considered to define the moments acting at the upper and lower arm joints for a simplified sequence for walking and running (George *et al.,* 2018). As expected, the results showed that the energy output during a simplified running vs. walking sequence was 2.06 mJ, compared to 0.42 mJ. The running sequence

as shown in Figure 3.7, will be considered when simulating the behavior of the harvester-generator model in this paper. To emulate the arm swing motion associated with running in the triple pendulum system, the time varying moments for the upper and lower arm joints $M_{E1}(t)$ and $M_{E2}(t)$, become

$$M_{E1}(t) = a\ sin(2\pi f t), \tag{3.10a}$$

$$a = (m_1 e_1 \sin\left(\frac{5\pi}{36}\right) + m_2\left(l_1 \sin\left(\frac{5\pi}{36}\right) + e_2 \sin\left(\frac{23\pi}{36}\right)\right) + m_3\left(l_1 \sin\left(\frac{5\pi}{36}\right) + l_2 \sin\left(\frac{23\pi}{36}\right)\right))g \tag{3.10b}$$

and

$$M_{E2}(t) = (m_2 e_2 + m_3 l_2)g \tag{3.10c}$$

The masses for the upper and lower arms are based on anthropomorphic data. Table 3.1 displays the parameter values for the mathematical model and prototype system.

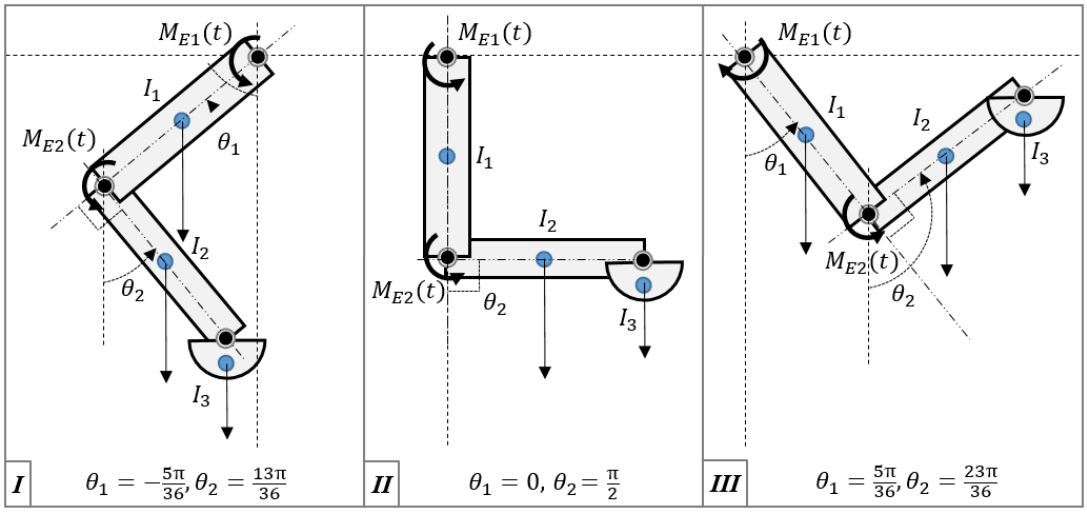

Figure 3.7: Sequence of running arm motion from positions I to III with an appropriate fixed angle of $\pi/2$ radians between the upper and lower arms.

Table 3.2. Summary of parameter values used in numerical study

Symbol	Value	Units	Symbol	Value	Units
c_1	1	N.m.s	k_T	1.53e-2	N.m.amp^{-1}
c_2	1	N.m.s	l_1	0.24	m
c_3	0.0025	N.m.s	l_2	0.25	m
C_G	1e-4	N.m.s	l_3	0.025	m
c_P	1e-5	N.m.s	L_G	0.63	H
e_1	0.12	m	m_1	2.63	kg
e_2	0.125	m	m_2	2.07	kg
e_3	0.0106	m	m_3	0.18	kg
f	2	Hz	N_{PG}	24	-
g	9.81	m s^{-2}	N_{RG}	120	-
I_1	0.05214	kg.m^2 .rad^{-1}	q_1	6.2478	N.m
I_2	0.04376	kg.m^2. rad^{-1}	q_2	2.9798	N.m
I_3	8.5182e-4	kg.m^2. rad^{-1}	r_1	0.05	m
I_P	5.625e-5	kg.m^2. rad^{-1}	r_2	0.035	m
I_{RG}	1.969e-5	kg.m^2. rad^{-1}	R_G	0.9	Ohm
I_{PG}	4.228e-9	kg.m^2. rad^{-1}	R_L	15	Ohm
J_G	3.103e-5	kg.m^2 rad^{-1}	R_T	15.9	Ohm
k_E	1.6e-2	V.rad^{-1}.sec^{-1}			

The system response of the energy harvester with respect to the prescribed arm inputs are displayed in Figure 8. The angular displacements for the upper and lower arms, refer to Figures 3.8b – 3.8c, closely resemble a typical arm swing motion during running per the input torque functions of Figure 3.8a. It should be noted that the triple pendulum system is somewhat chaotic in nature, and parameter value variations such as the damping constant may result in different behavior. The estimated voltage and current are plotted in Figure 8d which features peak values of 4V DC and 0.3 mA, respectively. The electric power, $P_E = R_G\, i_A{}^2 = R_G\, \dot{q}^2$, achieves a peak value of approximately 1.7 mW as illustrated in Figure 3.8e. The energy available over a representative 5 second period was 1.72 mJ which should be sufficient to help charge a small battery.

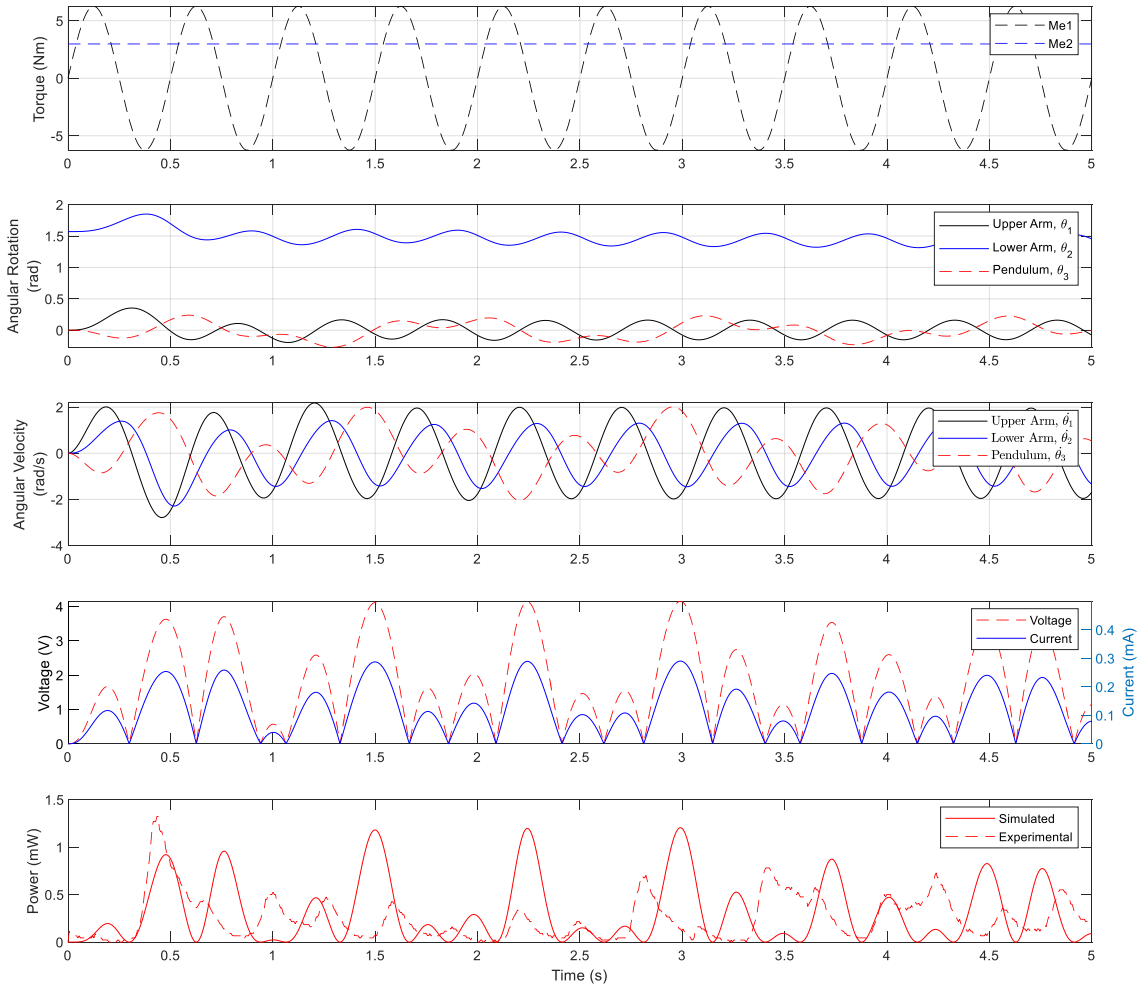

Figure 3.8: Numerical response of the energy harvester to prescribed running arm motion – (a) Input moments, (b) Pendula angular displacement, (c) Pendula angular velocity, and (d) DC Generator voltage and current, and (e) Generated electric power (dotted line corresponds to experimental data)

4.2 Experimental Results

The cadence and amplitude of an arm swing varies for each individual during walking and/or running activities. To gain initial insight into the behavior of the proposed harvester

in realistic conditions, its power output for human running was recorded. The author placed the device on their wrist and ran on a treadmill at a steady pace, attempting to approximately match a 2 Hz arm swing pace. Data was recorded separately for the two electrical modes for a 5 second time period. The unregulated mode output plotted in Figure 8e to compare with the simulated model results, produced a peak power output of 1.4 mW. The total energy generated was 1.39 mJ, which corresponds to 81% of the predicted output. The observed error may be partially attributed to the approximated generator constants in the mathematical model, and the effect of frictional forces in the prototype.

The power output from the wrist worn prototype harvester, in the regulated mode, has been displayed in Figure 3.9 for running. The measured output voltage and current remain essentially constant at 5V and 0.05A respectively. The peak power and energy generated were 0.25 mW and 1.16 mJ, which was 16% less than that from the unregulated supply. This may be explained by the nature of the boost converter which regulates the output by active switching operation based on the electrical input available. Nevertheless, the 5V DC output can be directly used to safely power electronic devices, unlike an unregulated supply. It is important to note that the LC circuit of the boost converter effectively decouples the load connection to the generator, resulting in a lower direct current draw from the generator, and thereby easier excitation of the harvester pendulum.

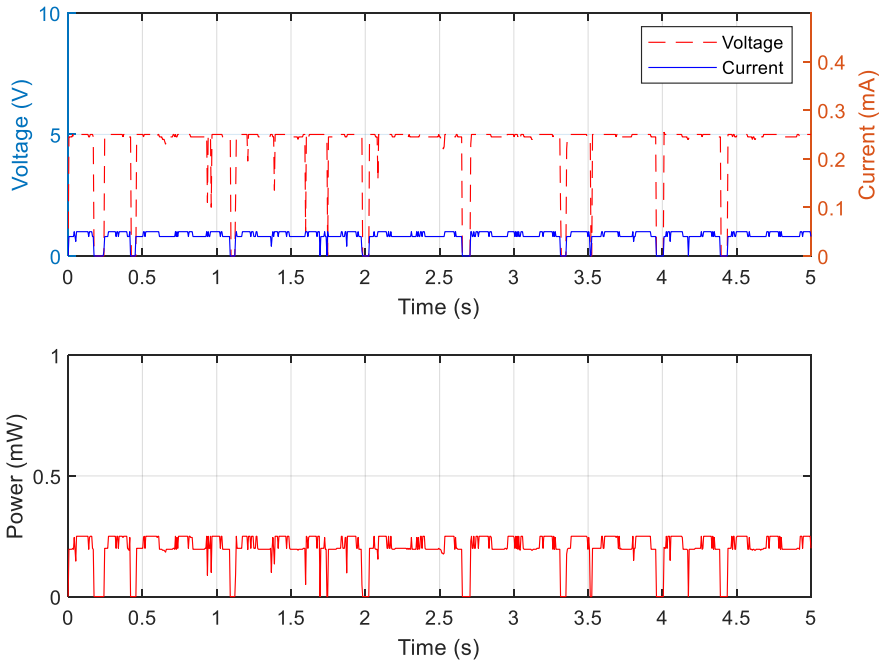

Figure 3.9: Experimental regulated mode DC generator output (measured after the boost converter) with a 1 kΩ resistive load as shown in Figure 3 – (a) Voltage and Current, and (b) Power

3.5 Summary

A wearable energy harvester was designed, fabricated and tested after evaluating the system performance through mathematical model based simulation study. The arm motion dynamics which emulated human running were an input to the triple pendulum system with coupled DC generator. The predicted harvester energy output was 1.72 mJ. In comparison, experimental testing of the prototype harvester yielded 67% (81%) of predicted output, corresponding to an energy output of 1.16 (1.39) mJ of energy in the regulated (unregulated) modes. The expected energy variations between the mathematical model and experimental system may be attributed to the input moments that excited the system. The

simulated input does not “react” to the changing behavior of the harvester, whereas in the real world, users involuntarily tend to input subtle variations in their arm swing to match motions of both arms. This action can induce a larger excitation in the harvester. The chaotic nature of the triple pendulum system could also provide a partial explanation behind the significant variation between the simulated and experimental values. Currently, the energy harvester requires excessive user motion to charge the onboard battery. Further research may be conducted to optimize the prototype by using a more efficient generator and power regulation technique such as active rectification.

CHAPTER FOUR

CONCLUSION

4.1 Results and Observations

A wearable energy harvester based on the autowinder mechanism has been designed, analyzed, fabricated and tested. Mathematical models based on a triple pendulum system were developed to understand the mechanical and electrical behavior of the system. The first model demonstrates the maximum mechanical energy generation potential of a harvester pendulum located at a user's wrist for activities of walking and running. A series of input torque was supplied to emulate these corresponding motions. The model predicted a maximum energy output of 0.42 mJ for walking and 2.06 mJ for running for a time period of 5 seconds. The second model considered the effects of the electromechanical system and a connected representative electrical load, and predicted the electrical energy output to be 1.72 mJ for running.

Experimental testing with electrical loads such as LED's, resistances and a Li-Po battery demonstrated an energy output of 1.39 mJ and 1.16 mJ, respectively, during unregulated and regulated modes. While the energy harvester demonstrated successful operation generating power with LED's and resistances under normal operation, it was observed that the harvester required a high degree of excitation, requiring vigorous shaking to charge a battery. This may be attributed to the DC generator's suitability for the application. It was also noted that the harvester exhibited inconsistent behavior under

various excitation frequencies and amplitudes, which may be explained due to the unpredictable and chaotic nature of the triple pendulum system.

4.2 Future Recommendations

The mathematical model was tuned with assumed values to emulate human arm motion during walking and running activities. The model assumed critical damping ratio for simulating the arm motion dynamics. Although the trajectory is comparable to real life arm motion, the assumed damping values may not fully represent the behavior of the arm-harvester system. The model accuracy may be improved with an appropriately designed control system with feedback for emulating human arm movement. By using constants that are specific to the user and the prototype, this model has the potential of predicting the prototype behavior with better accuracy.

The generator used in the prototype was a brushed industrial motor, rated to operate at high rpms in the range of 1000 to 3000. Average human arm swing ranges between 60 to 120 rpm, and the gear train implemented in the prototype has the potential of stepping up this frequency with a gear ratio of 1:5. Even though, this was not the ideal operating rpm range for the generator, since stepped up input would only be 600 rpm at the most. In future research, a Neodymium magnet based generator with a stronger magnetic field may be selected. This would enable a direct drive between the pendulum and the generator, reducing weight and transmission losses while improving power generation at low excitation frequencies.

The bridge rectifier used for converting alternating output of the generator into direct current has associated forward voltage losses during rectification, reducing the

energy harvested. Advanced rectification techniques such as active rectification utilizing efficient MOSFET switching may be used in the next version of the prototype, which decrease voltage losses significantly, down to a few mill volts. The commercial boost converter integrated in the prototype had a wide operating voltage range, which may have contributed to the high switching noise in the output. Furthermore, the capacitor and inductor used in the circuit are not well suited for the application. A boost converter circuit specifically designed for generator output range may be utilized for a smoother and consistent power supply.

The prototype successfully demonstrated the potential of human motion energy harvesting in a compact package. Future recommendations may be implemented to advance research towards a market ready consumer product. User-friendliness and ergonomics are important factors to be considered for successful consumer acceptance of the harvester, and hence, future research efforts may be undertaken towards designing a harvester with a smaller form factor. Comprehensive tests with wider range of subjects can provide insights into designing a harvester pendulum tuned for recurring excitation frequencies. Finally, future research may initiate collaboration with a commercial manufacturer, given the challenges in fabricating smaller components. Research towards, and the successful development of an energy harvester implemented with the proposed recommendations has the potential to create a significant positive impact on worldwide energy consumption and the current environmental scenario.

APPENDICES

Appendix A: Matlab Codes

Arm Dynamics and Harvester Response Simulation for Walking

```
%Triple Pendulum Equations of Motion by ABBY J GEORGE / Energy
Harvester
%Project
%Notes:
% Average Upper arm lengths = 236 to 245 mm ; Average Fore arm lengths
= 247mm - 251mm;
% Average Upper arm weights = 2.07 kg - 2.67 kg ; Average Fore arm
weights = 1.24 - 1.66 kg.
% OR USE Body weight %: - U.A. = 3.075%, L.A = 1.72%, H = 0.575%, L.A+H
= 2.295
% ==> [2.63 1.2 2.07] for 70kg
clear

m1 = 2.63; m2 = 2.07; m3 = .18;          % Masses (kg)
l1 = 0.24; l2 = 0.25; l3 = 0.025;        % Lengths (m)
e1 = l1/2; e2 = l2/2; e3 = 4*l3/(3*pi); % Mass center distances (m)
r1 = 0.05; r2 = 0.035;                   % Radii of approximated
cylindrical upper and lower arms (m)
g = 9.81;                                % Gravity (m.s-2)
c1 = 1; c2 = 1; c3 = 0;             % c = Damping const. (kg.m.s)
f1 = 0.7; f2 = 0.7;                        % 1 Hz = 2*pi rad/s
Time = 5;                                % Simulation Time (s)
Fine = 2000;                             % Number of divisions

% I1,I2 --> M.o.I for cylinder about the edge : (M*R^2)/4+(M*L^2)/3
(kg.m2)
% I3 --> M.o.I of half disk about center axis : M*R^2/2 (kg.m2)
I1 = vpa((m1*r1^2)/4 + (m1*l1^2)/3); I2 = vpa((m2*r2^2)/4 +
(m2*l2^2)/3); I3 = vpa((m3*l3^2)/2);

% From Equation (2.5)
L1 = m1*g*e1 + (m2 + m3)*g*l1;
L2 = m2*g*e2 + m3*g*l2;
L3 = m3*g*e3;

% From Equation (2.7)
A1 = I1 + (e1^2) * m1 + (l1^2) * (m2 + m3);
A2 = I2 + (e2^2) * m2 + (l2^2) * m3;
A3 = I3 + (e3^2) * m3;

% From Equation (2.7)
B12 = m2*e2*l1 + m3*l1*l2;
B13 = m3*e3*l1;
B23 = m3*e3*l2;

% Time vector
tVal = linspace(0,Time,Fine);
```

```
% Defining state vectors
syms x(t) y(t) z(t)
A = [x;y;z];

% From Equation (2.12a)
M = [A1 B12*cos(x-y) B13*cos(x-z);
B12*cos(x-y) A2 B23*cos(y-z);
B13*cos(x-z) B23*cos(y-z) A3];

% From Equation (2.12b)
N = [0 B12*sin(x-y) B13*sin(x-z);
-B12*sin(x-y) 0 B23*sin(y-z);
-B13*sin(x-z) -B23*sin(y-z) 0];

% From Equation (2.12c)
C = [c1+c2 -c2 0;
    -c2 c2+c3 -c3;
    0 -c3 c3];

% From Equation (2.12d)
p = [L1*sin(x);L2*sin(y);L3*sin(z)];

% <<<<<<<<<<<<<<<<<<<<<<<<<<<<<<<<<<<<<<<<<<<<<< ARM INPUTS (WALKING)
% 1 Hz = 2*pi rad/s
% Max Swing Angle for Upper & Lower Arm = 25 (deg)
deg = pi/180; rad = 180/pi;                  % conversions

% From Equations (2.14a) - (2.14d)
q1 = (m1*e1*sin(25*deg) + m2*(l1*sin(25*deg)+e2*sin((10+25)*deg)) +
m3*(l1*sin(25*deg)+l2*sin((10+25)*deg)))*g;
q2 = (m2*e2 + m3*l2)*g*sin((25+10)*deg);
Me1 = q1*sin(2*pi*f1*t);
Me2 = q2;

% From Equation (2.12e)
Fe = [Me1;Me2;0];

odes = (diff(A,t,2) == M\(Fe - p - C*diff(A,t) - N*(diff(A,t).^2)));
% Second Order to First Order
[V,S] = odeToVectorField(odes);

MV = matlabFunction(V,'Vars',{'t','Y'});

options = odeset('RelTol', 1e-10, 'AbsTol', 1e-12);

% y0 = Initial Values. S = [y; Dy; x; Dx; z; Dz]
y0 = [(10*deg) 0 0 0 0 0];
sol = ode45(MV,[0,Time],y0,options);

% storing solutions into yVal in the correct order
yVal = deval(sol,tVal,[3 1 5 4 2 6]);

% plots
```

```
figure('Name','Walking')
subplot(3,1,1)
yyaxis left
plot(tVal,(yVal(1,:)),'k-',tVal,(yVal(2,:)),'r-')
ylabel({'Angular Displacement';'(degrees)'})
yyaxis right
fplot(Me1,[0 Time],'k--')
hold on
fplot(Me2,[0 Time],'r--')
legend('Upper Arm','Lower Arm', 'Me1','Me2')
ylabel('Torque(Nm)')
grid;

subplot(3,1,2)
plot(tVal,yVal(4,:),'k-',tVal,yVal(5,:),'r-',tVal,yVal(6,:),'b--')
legend('Upper Arm','Lower Arm','Pendulum')
ylabel({'Angular Velocity';'(rad/s)'})
grid;
%Maximum Power output in Watts -> T * w // T = I3 * acc * Dz
%Energy Harvested = Average power * Time

subplot(3,1,3)
% Differentiating Proof mass Velocity
acc = abs([0 diff(yVal(6,:))]);
m_Power_mW = I3 * acc .* abs(yVal(6,:))*1000;     % Power in mW
plot(tVal,m_Power_mW,'b-')
xlabel('Time (s)');
ylabel('Power (mW)');
m_Energy_mJ = double(sum(m_Power_mW)*(1/length(tVal)))*Time
grid;
```

Arm Dynamics and Harvester Response Simulation for Running

```
%Triple Pendulum Equations of Motion by ABBY J GEORGE / Energy
Harvester
%Project
%Notes:
% Average Upper arm lengths = 236 to 245 mm ; Average Fore arm lengths
= 247mm - 251mm;
% Average Upper arm weights = 2.07 kg - 2.67 kg ; Average Fore arm
weights = 1.24 - 1.66 kg.
% OR USE Body weight %: - U.A. = 3.075%, L.A = 1.72%, H = 0.575%, L.A+H
= 2.295
% ==> [2.63 1.2 2.07] for 70kg
clear

m1 = 2.63; m2 = 2.07; m3 = 0.18;          % Masses (kg)
l1 = 0.24; l2 = 0.25; l3 = 0.025;        % Lengths (m)
e1 = l1/2; e2 = l2/2; e3 = 4*l3/(3*pi); % Mass center distances (m)
r1 = 0.05; r2 = 0.035;                   % Radii of appproximated
cylindrical upper and lower arms (m)
g = 9.81;                                % Gravity (m.s-2)
c1 = 1; c2 = 1; c3 = 0;             % c = Damping const. (kg.m.s)
f1 = 2; f2 = 2;                          % 4 Hz = 8*pi rad/s
Time = 5;                                % Simulation Time (s)
Fine = 2000;                             % Number of divisions

% I1,I2 --> M.o.I for cylinder about the edge : (M*R^2)/4+(M*L^2)/3
(kg.m2)
% I3 --> M.o.I of half disk about center axis : M*R^2/2 (kg.m2)
I1 = vpa((m1*r1^2)/4 + (m1*l1^2)/3); I2 = vpa((m2*r2^2)/4 +
(m2*l2^2)/3); I3 = vpa((m3*l3^2)/2);

% From Equation (2.5)
L1 = m1*g*e1 + (m2 + m3)*g*l1;
L2 = m2*g*e2 + m3*g*l2;
L3 = m3*g*e3;

% From Equation (2.7)
A1 = I1 + (e1^2) * m1 + (l1^2) * (m2 + m3);
A2 = I2 + (e2^2) * m2 + (l2^2) * m3;
A3 = I3 + (e3^2) * m3;

% From Equation (2.7)
B12 = m2*e2*l1 + m3*l1*l2;
B13 = m3*e3*l1;
B23 = m3*e3*l2;

% Time vector
tVal = linspace(0,Time,Fine);

% Defining state vectors
syms x(t) y(t) z(t)
A = [x;y;z];
```

```
% From Equation (2.12a)
M = [A1 B12*cos(x-y) B13*cos(x-z);
B12*cos(x-y) A2 B23*cos(y-z);
B13*cos(x-z) B23*cos(y-z) A3];

% From Equation (2.12b)
N = [0 B12*sin(x-y) B13*sin(x-z);
-B12*sin(x-y) 0 B23*sin(y-z);
-B13*sin(x-z) -B23*sin(y-z) 0];

% From Equation (2.12c)
C = [c1+c2 -c2 0;
    -c2 c2+c3 -c3;
    0 -c3 c3];

% From Equation (2.12d)
p = [L1*sin(x);L2*sin(y);L3*sin(z)];

% <<<<<<<<<<<<<<<<<<<<<<<<<<<<<<<<<<<<<<<<<<<<<< ARM INPUTS (RUNNING)
% 4 Hz = 8*pi rad/s
% Max Angle for Upper Arm = 25 (deg),Constant Lower Arm Angle = 90
(deg)
deg = pi/180;rad = 180/pi;                                % conversions

% From Equations (2.15a) - (2.14d)
q1 = (m1*e1*sin(25*deg) +
m2*(l1*sin(25*deg)+e2*sin((90+25)*deg))+m3*(l1*sin(25*deg)+l2*sin((90+2
5)*deg)))*g;
q2 = (m2*e2 + m3*l2)*g;
Me1 = q1*sin(2*pi*f1*t);
Me2 = q2;

% From Equation (2.12e)
Fe = [Me1;Me2;0];

odes = (diff(A,t,2) == M\(Fe - p - C*diff(A,t) - N*(diff(A,t).^2)));
[V,S] = odeToVectorField(odes);
% Second Order to First Order
MV = matlabFunction(V,'Vars',{'t','Y'});

% y0 = Initial Values. S = [y; Dy; x; Dx; z; Dz]
y0 = [(90*deg) 0 0 0 0 0];
sol = ode45(MV,[0,Time],y0);

% storing solutions into yVal in the correct order
yVal = deval(sol,tVal,[3 1 5 4 2 6]);

% plots
figure('Name','Running')
subplot(3,1,1)
yyaxis left
plot(tVal,(yVal(1,:)),'k-',tVal,(yVal(2,:)),'r-')
ylabel({'Angular Displacement';'(degrees)'})
```

```
yyaxis right
fplot(Me1,[0 Time],'k--')
hold on
fplot(Me2,[0 Time],'r--')
legend('Upper Arm','Lower Arm', 'Me1','Me2')
ylabel('Torque(Nm)')
grid;

subplot(3,1,2)
plot(tVal,yVal(4,:),'k-',tVal,yVal(5,:),'r-',tVal,yVal(6,:),'b--')
legend('Upper Arm','Lower Arm','Pendulum')
ylabel({'Angular Velocity';'(rad/s)'})
grid;

%Maximum Power output in Watts -> T * w // T = I3 * acc * Dz
%Energy Harvested = Average power * Time

subplot(3,1,3)
% Differentiating Proof mass Velocity
acc = abs([0 diff(yVal(6,:))]);
m_Power_mW = I3 * acc .* abs(yVal(6,:))*1000;     % Power in mW
m_Energy_mJ = double(sum(m_Power_mW)*(1/length(m_Power_mW)))*Time
plot(tVal,m_Power_mW,'b')
xlabel('Time (s)');
ylabel('Power (mW)');
%print('Instantaneous Power','-djpeg','-r300');
grid;
```

Harvester-Generator Model Simulation for Running

```
%Triple Pendulum Equations of Motion by ABBY J GEORGE / Energy
Harvester
%Project
%Notes:
% Average Upper arm lengths = 236 to 245 mm ; Average Fore arm lengths
= 247mm - 251mm;
% Average Upper arm weights = 2.07 kg - 2.67 kg ; Average Fore arm
weights = 1.24 - 1.66 kg.
% OR USE Body weight %: - U.A. = 3.075%, L.A = 1.72%, H = 0.575%, L.A+H
= 2.295
% ==> [2.63 1.2 2.07] for 70kg

clear

% MODEL PARAMETERS
g = 9.81;
% Damping constants (kg.m.s)
c1 = 1; c2 = 1; c_p = 0.00001; Cg = 0.0001;
% Excitation frequency (1 Hz = 2*pi rad/s)
f1 = 2; f2 = 2;
% Gear Ratio
Nrg = 120; Npg = 24; GR = Nrg/Npg;
% Generator Constants
Kt = 0.0153;
Ke = 2*0.0067415;
Lg = 0.63;
Ra = 0.9;
Rl = 10;
% Simulation Time (s), Resolution
Time = 5; Fine = 2000;

% ###MASSES (kg)
% Pendula
m1 = 2.63; m2 = 2.07; m3 = 0.18;
% Ring & Pinion gears
m_rg = vpa(0.0110986753); m_pg = vpa(0.000209758072);
% Generator
m_g = vpa(0.042753358);

% ###LENGTHS (m)
% Pendulum (1,2,3)
l1 = 0.24; l2 = 0.25; l3 = 0.025;
% Ring & Pinion gears, Generator
r_out_rg = vpa(0.0507492); r_in_rg = vpa(0.0312166); r_pg =
vpa(0.00635);r_g = vpa(0.0381);
% Mass centers of the pendulum
e1 = l1/2; e2 = l2/2; e3 = 4*l3/(3*pi);
% Radii of cylindrical upper and lower arms
r1 = 0.05; r2 = 0.035;
```

```
% ###INERTIAS
% I1,I2 --> M.o.I for cylinder along edge : (M*R^2)/4+(M*L^2)/3
% Ip = MoI of Pendulum: 0.5*M*R^2
% Irg = MoI of Ring Gear: 0.5*M*(R1^2 - R2^2)
% Ipg = MoI of Pinion Gear: 0.5*M*R^2
% Pendulum (1,2,p)
I1 = vpa((m1*r1^2)/4 + (m1*l1^2)/3);
I2 = vpa((m2*r2^2)/4 + (m2*l2^2)/3);
Ip = vpa((m3*l3^2)/2);
% Gears (Ring, Pinion)
Irg = vpa(0.5*m_rg*(r_out_rg^2 + r_in_rg^2));
Ipg = vpa(0.5*m_pg*(r_pg^2));
% Generator
Jg = vpa(0.5*m_g*(r_g^2));

% Pendulum Inertia coupled to DC Generator thru gear train
I3 = vpa(Ip + Irg + ((Nrg/Npg)^2)*(Ipg + Jg));

% Damping effect coupled through gear train
c3 = c_p + ((Nrg/Npg)^2)*Cg;

% From Equation (3.3)
U1 = m1*g*e1 + (m2 + m3)*g*l1;
U2 = m2*g*e2 + m3*g*l2;
U3 = m3*g*e3;

% From Equation (3.3)
A1 = I1 + (e1^2) * m1 + (l1^2) * (m2 + m3);
A2 = I2 + (e2^2) * m2 + (l2^2) * m3;
A3 = I3 + (e3^2) * m3;

% From Equation (3.3)
B12 = m2*e2*l1 + m3*l1*l2;
B13 = m3*e3*l1;
B23 = m3*e3*l2;

% Time vector
tVal = linspace(0,Time,Fine);

% Defining state vectors
syms x(t) y(t) z(t) q(t)
A = [x;y;z;q];

% From Equation (3.9a)
M = [A1 B12*cos(x-y) B13*cos(x-z) 0;
B12*cos(x-y) A2 B23*cos(y-z) 0;
B13*cos(x-z) B23*cos(y-z) A3 0;
0 0 0 Lg];

% From Equation (3.9b)
N = [0 B12*sin(x-y) B13*sin(x-z) 0;
-B12*sin(x-y) 0 B23*sin(y-z) 0;
-B13*sin(x-z) -B23*sin(y-z) 0 0;
```

```
0 0 0 0];

% From Equation (3.9c)
C = [c1+c2 -c2 0 0;
    -c2 c2+c3 -c3 0;
    0 -c3 c3 (Npg/Nrg)*Kt;
    0 0 -Ke*(Nrg/Npg) Ra+Rl];

% From Equation (3.9d)
p = [U1*sin(x);U2*sin(y);U3*sin(z);0];

% ARM INPUTS (WALKING)
% 1 Hz = 2*pi rad/s
% Max Swing Angle for Upper & Lower Arm = 25 (deg)
deg = pi/180; rad = 180/pi;                  % conversions

% From Equation (3.10a)- (3.10c)
q1 = (m1*e1*sin(25*deg) +
m2*(l1*sin(25*deg)+e2*sin((90+25)*deg))+m3*(l1*sin(25*deg)+l2*sin((90+2
5)*deg)))*g;
q2 = (m2*e2 + m3*l2)*g;
Me1 = q1*sin(2*pi*f1*t);
Me2 = q2;

% From Equation (3.9e)
Fe = [Me1;Me2;0;0];

odes = (diff(A,t,2) == M\(Fe - p - C*diff(A,t) - N*(diff(A,t).^2)));
% Triple Pendulum ODE

[V,S] = odeToVectorField(odes);                                          %
Second Order to First Order
MV = matlabFunction(V,'Vars',{'t','Y'});

% y0 = Initial Values. S = [y; Dy; x; Dx; z; Dz; q; Dq]

options = odeset('RelTol', 1e-10, 'AbsTol', 1e-12);

y0 = [(90*deg) 0 0 0 0 0 0 0];
sol = ode45(MV,[0,Time],y0,options);
yVal = deval(sol,tVal,[3 1 5 4 2 6 7 8]);

% Plots
figure('Name','Harvester')
subplot(4,1,1)
fplot(Me1,[0 Time],'k--')
hold on
fplot(Me2,[0 Time],'b--')
legend('Me1','Me2')
ylabel('Torque(Nm)')
grid;
```

```
subplot(4,1,2)
plot(tVal,(yVal(1,:)),'k-',tVal,(yVal(2,:)),'b-',tVal,(yVal(3,:)),'r--
')
ylabel({'Angular Rotation';'(rad)'})
legend('Upper Arm, \theta_{1}','Lower Arm, \theta_{2}','Pendulum,
\theta_{3}')
grid;

subplot(4,1,3)
plot(tVal,yVal(4,:),'k-',tVal,yVal(5,:),'b-',tVal,yVal(6,:),'r--')
legend('Upper Arm, $\dot{\theta_{1}}$','Lower Arm,
$\dot{\theta_{2}}$','Pendulum,
$\dot{\theta_{3}}$','interpreter','latex')
ylabel({'Angular Velocity';'(rad/s)'})
grid;
%Maximum Power output in Watts -> T * w // T = I3 * acc * Dz
%Energy Harvested = Average power * Time

% subplot(3,1,3)
% grid on;
acc = abs([0 diff(yVal(6,:))]);             % Differentiating Proof
mass Velocity
m_Power_mW = I3 * acc .* abs(yVal(6,:))*1000;    % Power in mW
% plot(tVal,mPower,'b-')
% xlabel('Time (s)');
% ylabel('Power (mW)');
m_Energy_mJ= double(sum(m_Power_mW)*(1/length(m_Power_mW)))*Time

subplot(4,1,4)                                                  % Power =
I^2 * R
e_Power_mW = (abs(yVal(8,:)).*(abs(yVal(8,:))))*(Ra + Rl)*1000;
e_Energy_mJ = double(sum(e_Power_mW)*(1/length(e_Power_mW)))*Time
plot(tVal,e_Power_mW,'r-')
xlabel('Time (s)');
ylabel('Power (mW)');
%yyaxis right
%plot(tVal,yVal(3,:),'b-')
%ylabel('Harvester displacement')
%legend('Power','Displacement')
grid;
Volts = yVal(8,:).*(Ra+Rl);
figure
plot(tVal,Volts)
```

Matlab WiFi Client for datalogging

```
close;
clear;

pause(2)

% Connect to IP Address and port number, create MATLAB tcpclient object
client = tcpclient('192.168.137.9', 80);

% Pause for harvester excitation
pause(6)

% Read data from client
data = read(client);
Time = 5; % Seconds

% creating zero vectors
Voltage = zeros;
Current = zeros;
Power = zeros;

% Sorting data into voltage and current
j = 0; m = 0;

for i = 1:2:length(data)
    j = j+1;
Voltage(1,j)= data(i);
end

for k = 2:2:length(data)
m = m+1;
Current(1,m)=data(k);
end

tVal = (0:(Time/length(Voltage)):Time);

% conversion

V = 0.1*Voltage; % Voltage conversion from Arduino (V)
I = 0.1*Current; % Current conversion from Arduino (A), I = 0.01*I;
power = V .*I; % Power in mW

% Plots
subplot(2,1,1)
xlabel('Time (s)');
yyaxis left
plot(tVal,[0 V],'r--')
ylabel('Voltage (V)');
axis([0 5 0 10]);
yyaxis right
```

```
plot(tVal,[0 I],'b-')
ylabel('Current (mA)');
axis([0 5 0 10]);
legend('Voltage','Current');
grid;

subplot(2,1,2)
plot(tVal,[0 power],'r-')
xlabel('Time (s)');
ylabel('Power (mW)');
axis([0 5 0 1]);
grid;
E_Energy_mJ = double(sum(power)*(1/length(tVal)))*Time % Energy in mJ
```

Appendix B: Arduino Code for Data Logging

```
#include <WiFi.h>
#include <Wire.h>
#include <Adafruit_INA219.h>
const char* ssid     = "4ESP32"; // WiFi network/hotspot name
const char* password = "GoTigers2018"; // Network SSID
WiFiServer server(80); // initialize server on port 80
Adafruit_INA219 ina219; // initialize INA219 current sensor
void setup() // main loop
{
   Serial.begin(115200);
   Serial.println();
   Serial.println();
   WiFi.begin(ssid, password);
   while (WiFi.status() != WL_CONNECTED)
   {
      delay(200);
      Serial.print(".");
   }
   Serial.println("");
   Serial.println("WiFi connected to IP address:");
   Serial.println(WiFi.localIP());
```

```
   server.begin();
   uint32_t currentFrequency;
   ina219.begin(); // begin communication
   ina219.setCalibration_16V_400mA(); // ina219 accuracy setting
}
int value = 0;
void loop()
{
 WiFiClient client = server.available();
 if (client)
 {
   if (client.connected())
   {
     Serial.println("Client Connected");
     int t1 = millis();
     delay(100);
     int i = millis();
     while(i-t1<=5100)
     {
       i = millis();

       float busvoltage = 0;
```

```
        float current_mA = 0;
        float shuntvoltage = 0;
        float loadvoltage = 0;
        int V = 0;
        int I = 0;
        shuntvoltage = ina219.getShuntVoltage_mV();
        busvoltage = ina219.getBusVoltage_V();
        current_mA = ina219.getCurrent_mA();
        loadvoltage = busvoltage + shuntvoltage/1000;
       V = loadvoltage*10; // value sent is one byte, shifting decimal
       I = current_mA*10;
        client.write(V); // write value to client
        client.write(I);
       }
    }
  }
}
```

Appendix C: Photographs of Energy Harvester Components

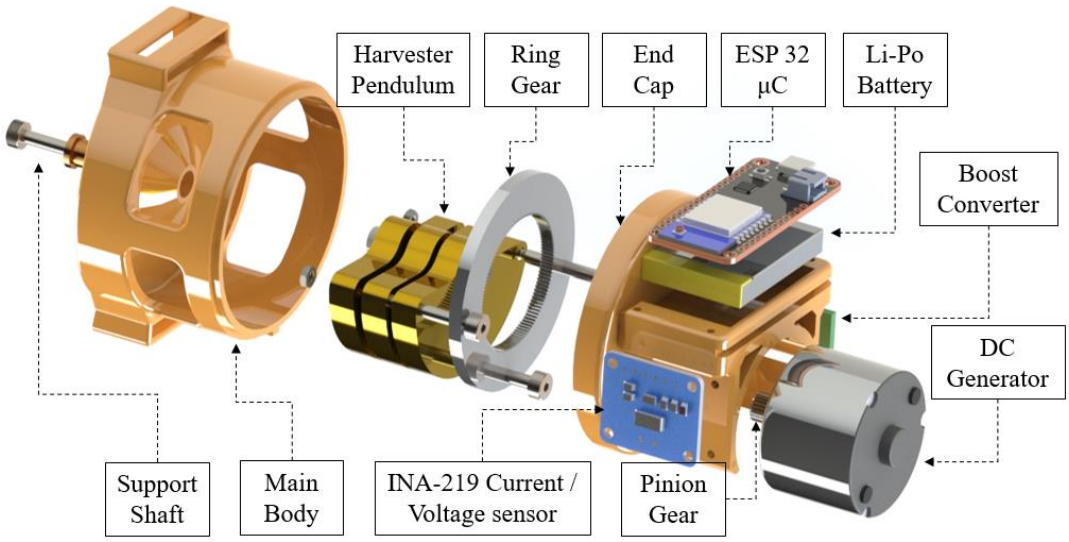

Figure C-1. CAD rendering showing disassembled energy harvester

Figure C-2. CAD rendering showing assembled energy harvester

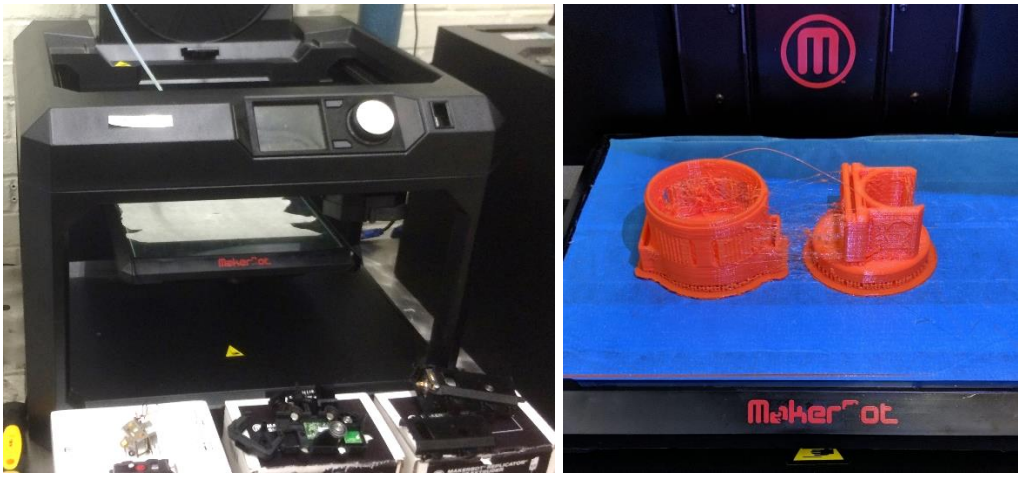

Figure C-3. Photograph showing (a) Makerbot 3-D printer and, (b) 3-D printed harvester enclosure

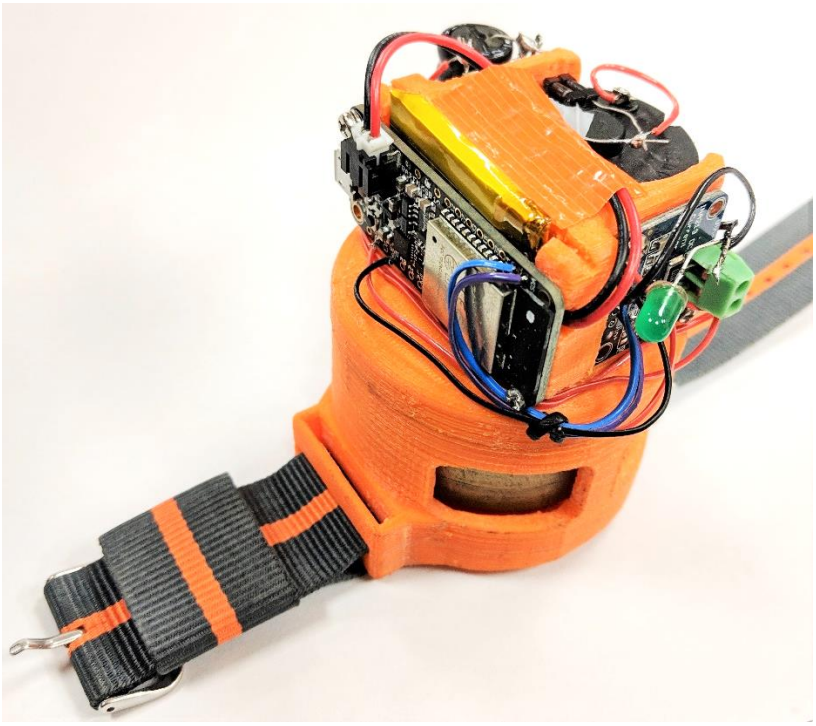

Figure C-4. Photograph of the assembled energy harvester

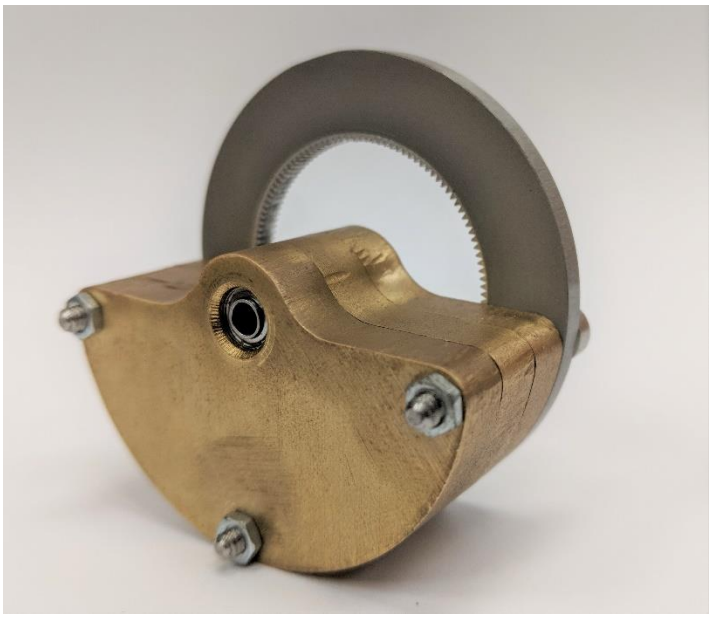

Figure C-5. Photograph of the coupled harvester pendulum and ring gear

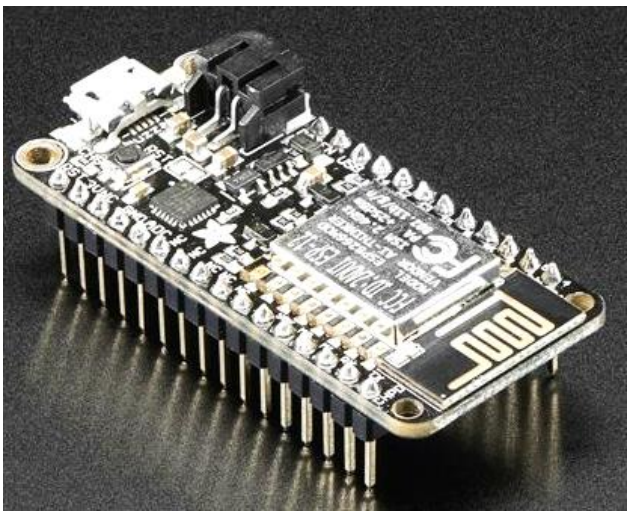

Figure C-6. Photograph of the ESP 32 Microcontroller

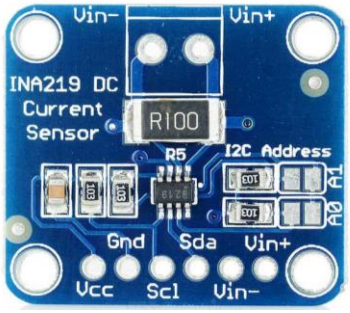

Figure C-7. Photograph of the INA-219 Current sensor

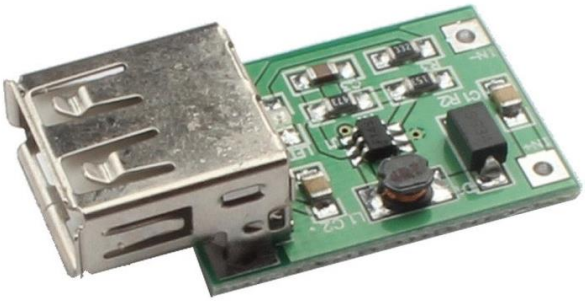

Figure C-8. Photograph of the 5VDC Boost converter

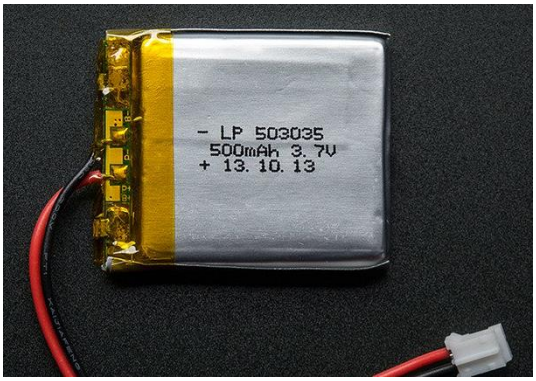

Figure C-9. Photograph of the 500 mAh LiPo battery

Appendix D: Bill of Materials

No.	Item	#	Unit Price	Source /Link
1	24 T Sun Gear	1	$19.22	http://shop.sdp-si.com/catalog/product/?id=S1043Z-096A024
2	Bearings (For Sun/Planet)	2	$10.97	https://www.mcmaster.com/#57155k339/=1byvgqm
3	50 T Planet Gear	1	$15.34	http://shop.sdp-si.com/catalog/product/?id=S1063Z-096A050
4	120 T Ring Gear	1	$72.72	http://shop.sdp-si.com/catalog/product/?id=S1E62Z-096A120
5	Brass Bar (For Pendulum)	1	$29.96	https://www.mcmaster.com/#1784N13
6	Connecting Shaft	1	$7.82	https://www.ondrivesus.com/cds_catalog_product.php?id=GTM1000-100
7	Bearings: (For Pendulum)	2	$5.67	https://www.mcmaster.com/#57155K382
8	Main Shaft	1	$9.29	https://www.mcmaster.com/#1263k39/=17511dx
9	Enclosure	1	$0	3-D printed at Cook Engineering Laboratory
10	Shoulder screw 7/8”	3	$2.75	https://www.mcmaster.com/#94035a139/=1ccdqft
11	Shoulder screw 1”	1	$2.40	https://www.mcmaster.com/#91327a286/=1cgdmb0
12	Narrow Hex Nut	1	$2.36	https://www.mcmaster.com/#90760a005/=1cgfmr6
13	Flanged Sleeve Bearing	1	$0.66	https://www.mcmaster.com/#6338k561/=1csp4mm

14	Adafruit ESP32 Microcontroller	1	$19.95	https://www.adafruit.com/product/3405
15	Boost Converter	1	$10.00	https://www.amazon.com/DAOKI-Control-Converter-Charger-0-9V-5V/dp/B00XT0PEAO
16	INA-219 Current Sensor	1	$7.99	https://www.amazon.com/KNACRO-INA219-Bi-directional-Current-Monitor/dp/B01HXNMSDS
17	DC Generator	1	N/A	https://www.hsiangneng.com/HN-35GA.htm
18	Schottky Diodes	4	$6.79	https://www.amazon.com/AKOAK-Schottky-Blocking-Diodes-15SQ045/dp/B01CXOQMJ8
19	500 mAh Lithium Ion Battery	1	$12.79	https://www.amazon.com/gp/product/B00L0W61VO
20	Watch Strap	1	$11.85	hhttps://www.amazon.com/BARTON-Watch-Bands-Pumpkin-Version/dp/B01E62WO6K

REFERENCES

Beeby, S., Tudor, M., and White, N., "Energy Harvesting Vibration Sources for Microsystems Applications," Measurement Science and Technology, vol. 17, no. 12, pp. R175–R195, 2006.

BP Statistical review of world energy, "https://www.bp.com/content/dam/bp/en/-corporate/pdf/energy-economics/statistical-review/bp-stats-review-2018-full-report.pdf ," accessed on 12/15/2018.

Breguet, E., and Chapman, M., "Breguet: Art and Innovation in Watchmaking," Munich: Prestel Publishing, October 2015.

Bruijn, S. M., Meijer, O. G., van Dieen, J. H., Kingma, I., and Lamoth, C. J. C., "Coordination of Leg Swing, Thorax Rotations, and Pelvis Rotations During Gait: The Organization of Total Body Angular Momentum," Gait Posture, vol. 27, pp. 455–462, 2008.

Burdet, E., Osu, R., Franklin, D.W., Yoshioka, T., Milner, T.E., and Kawato, M., "A Method for Measuring Endpoint Stiffness During Multi-Joint Arm Movements," Journal of Biomechanics, vol. 33, pp. 1705 – 1709, 2000.

Business Insider, "https://www.businessinsider.com/world-population-mobile-devices-2017-9," accessed on 12/15/2018.

Callaway, E. H., "Wireless Sensor Networks: Architectures and Protocols," Boca Raton: Auerbach Publications, August 2003.

Collins, S.H., Adamczyk, P.G., and Kuo, A.D., "Dynamic Arm Swinging in Human Walking," Proceedings of the Royal Society B, vol. 276, pp. 3679-3699, 2009.

David, A.W., "Biomechanics and Motor Control of Human Movement," 4th Edition, John Wiley & Sons Inc., Hoboken, 2009

Donelan, J. M., Naing, V., Hoffer, J. A., Weber, D. J., and Kuo, A. D., "Biomechanical Energy Harvesting: Generating Electricity During Walking with Minimal User Effort," Science, vol. 319, Issue 5864, pp. 807–810, 2008.

Elftman, H., "The Function of Arms in Walking," Human Biology, vol. 11, pp. 529–535, 1939.

Fry, D. N., Wintenberg, A. L., and Bryan, B. L., "Integrated Power Management for Microsystems," proceedings of the Prospector IX: Human Powered Systems Technologies Workshop, Durham, NC, pp. 348-350, 1997.

George, A. J., Moline, D., and Wagner, J., "Arm Motion Dynamics to Excite a Mobile Energy Harvesting Autowinder," Technical Report, Department of Mechanical Engineering, Clemson University, Clemson, SC, November 2018.

Green, P.L., Papatheou, E., Sims, N.D., "Energy Harvesting from Human Motion and Bridge Vibrations: An Evaluation of Current Nonlinear Energy Harvesting Solutions," Journal of Intelligent Material Systems and Structures, vol. 24, pp. 1494-1505, 2013.

Hama, N., Yajima, A., Yoshida, Y., Utsunomiya, F., Kodate, J., Tsukahara, T., and Douseki, T., "SOI Circuit Technology for Batteryless Mobile System with Green Energy Sources," *IEEE Symposium on VLSI Circuits Digest of Technical Papers,* pp. 280-283, 2002.

Herr, H., and Popovic, M. "Angular Momentum in Human Walking," Journal of Experimental Biology, vol. 211, pp. 467–481, 2008.

Jackson, K. M., Joseph, J., and Wyard, S. J. "The Upper Limbs During Human Walking Part 2: Function," Electromyography and Clinical Neurophysiology, vol. 23, pp. 435–446, 1983.

Jansen, A., and Stevels, A., "Combining Eco-Design and User Benefits from Human-powered Energy Systems, a Win-Win Situation," *Journal of Cleaner Production,* vol. 14, no. 15-16, pp. 1299 – 1306, 2006.

K-Tor USB Hand Crank Generator, “https://www.k-tor.com/usb-hand-crank-generator,” accessed on 12/15/2018.

Meninger, S., Mur-Miranda, J.O., Amirtharajah, R., Chandrakasan, A.P., and Lang, J.H., “Vibration-to-Electric Energy Conversion,” *IEEE Transactions on Very Large Scale Integration (VLSI) Systems*, vol. 9, no. 1, pp. 64-76, 2001.

Mitcheson, P.D., Rao, G.K., and Green, T.C., “Energy Harvesting From Human and Machine Motion for Wireless Electronic Devices,” Proceedings of the IEEE, vol. 96, no. 9, pp. 1457-1486, 2008.

Omega SA, https://www.omegawatches.com/en-us/watch-omega-speedmaster-moonwatch-omega-co-axial-chronograph-44-25-mm-31130445101002, accessed on 12/15/2018.

Ortega, J. D., Fehlman, L. A., and Farley, C. T. “Effects of Aging and Arm Swing on the Metabolic Cost of Stability in Human Walking,” Journal of Biomechanics, vol. 41, pp. 3303–3308, 2008.

Pillatsch, P., Yeatman, E.M., and Holmes, A.S., “A Piezoelectric Frequency Up-converting Energy Harvester with Rotating Proof Mass for Human Body Applications,” Sensors and Actuators A:Physical, vol. 206, pp. 178-185, 2014.

Poulin, G., Sarraute, E., and Costa, F., “Generation of Electrical Energy for Portable Devices Comparative Study of an Electromagnetic and a Piezoelectric System,” *Sensors and Actuators A: Physical*, vol. 114, no. 3, pp. 461-471, 2004.

RavPower solar charger, “https://www.ravpower.com/p/ravpower-15000mah-solar-power-bank.html,” accessed on 12/15/2018.

Rome, L., Flynn, L., Goldman, E. M., and Yoo, T. D., “Generating Electricity While Walking with Loads,” Science, vol. 309, Issue 5741, pp. 1725–172, 2005.

Saha, C.R., O'Donnel, T., Wang, N., and McCloskey, P., "Electromagnetic Generator for Harvesting Energy from Human Motion," *Sensors and Actuators A: Physical*, vol. 147, no. 1, pp. 248-253, 2008.

Sato, N., Ishii, H., Urano, M., Sakata, T., Terada, J., Morimura, H., Shige-Matsu, S., Kudou, K., Kamei, T., and Machida, K., "Novel MEMS Power Generator With Integrated Thermoelectric and Vibrational Devices," Proceedings of the 13th International Conference on Solid-State Sensors, Actuators and Microsystems, pp. 295–298, Seoul, South Korea, 2005.

Seiko Watch Corporation, "https://museum.seiko.co.jp/en/collections/clock_watch/category3/collect041.html," accessed on 12/15/2018.

Shenck, N. S., and Paradiso, J. A., "Energy Scavenging with Shoe-Mounted Piezoelectrics," IEEE Micro, vol. 21, no.3, pp. 30–42, 2001.

Starner, T., "Human Powered Wearable Computing," IBM Systems Journal, vol. 35, no. 3&4, 1996.

Turri, S., Miller, D., Ben Ahmed, H., and Multon, B., "Design of an Electro-Mechanical Portable System Using Natural Human Body Movements for Electricity Generation," European Power Electronics and Drive Journal, vol. 13, pp.10, Toulouse, France, 2003.

Umberger, B. "Effects of Suppressing Arm Swing on Kinematics, Kinetics, and Energetics of Human Walking," Journal of Biomechanics, vol. 41, pp. 2575–2580, 2008.

Wang, J., Wang, W., Jewell, G.W., and Howe, D., "Design of a Miniature Permanent-Magnet Generator and Energy Storage System," IEEE Transactions on Industrial Electronics, vol. 52, no. 5, pp. 1383-1390, October 2005

Xie, L., Menet, C.G., Ching, H., and Du, R., "The Automatic Winding Device of a Mechanical Watch Movement and Its Application in Energy Harvesting," Journal of Mechanical Design, vol. 131, 071005-1, 2009.

Yun, J., Patel, S.N., Reynolds, M.S., and Abowd, G.D., “Design and Performance of an Optimal Inertial Power Harvester for Human-Powered Devices,” IEEE Transactions on Mobile Computing, vol. 10, no. 5, pp. 669-683, May 2011.